Redox Biology 50 (2022) 102240

Contents lists available at ScienceDirect

Redox Biology

journal homepage: www.elsevier.com/locate/redox

Secretory pathway Ca^{2+}-ATPase SPCA2 regulates mitochondrial respiration and DNA damage response through store-independent calcium entry

Monish Ram Makena [a], Myungjun Ko [a], Allatah X. Mekile [a], Nanami Senoo [a], Donna K. Dang [b], John Warrington [c], Phillip Buckhaults [c], C. Conover Talbot Jr. [d], Steven M. Claypool [a], Rajini Rao [a,*]

[a] Department of Physiology, Johns Hopkins University School of Medicine, Baltimore, MD, USA
[b] Vanderbilt University, Nashville, TN, USA
[c] Department of Drug Discovery and Biomedical Sciences, College of Pharmacy, University of South Carolina, Columbia, SC, USA
[d] Institute for Basic Biomedical Sciences, Johns Hopkins University School of Medicine, Baltimore, MD, USA

ARTICLE INFO

Keywords:
Ca^{2+} signaling
p53
ROS
Mitochondria
Doxorubicin
Oxygen consumption rate
DNA damage Response
ER+ breast cancer

ABSTRACT

A complex interplay between the extracellular space, cytoplasm and individual organelles modulates Ca^{2+} signaling to impact all aspects of cell fate and function. In recent years, the molecular machinery linking endoplasmic reticulum stores to plasma membrane Ca^{2+} entry has been defined. However, the mechanism and pathophysiological relevance of store-independent modes of Ca^{2+} entry remain poorly understood. Here, we describe how the secretory pathway Ca^{2+}-ATPase SPCA2 promotes cell cycle progression and survival by activating store-independent Ca^{2+} entry through plasma membrane Orai1 channels in mammary epithelial cells. Silencing SPCA2 expression or briefly removing extracellular Ca^{2+} increased mitochondrial ROS production, DNA damage and activation of the ATM/ATR-p53 axis leading to G0/G1 phase cell cycle arrest and apoptosis. Consistent with these findings, SPCA2 knockdown confers redox stress and chemosensitivity to DNA damaging agents. Unexpectedly, SPCA2-mediated Ca^{2+} entry into mitochondria is required for optimal cellular respiration and the generation of mitochondrial membrane potential. In hormone receptor positive (ER+/PR+) breast cancer subtypes, SPCA2 levels are high and correlate with poor survival prognosis. We suggest that elevated SPCA2 expression could drive pro-survival and chemotherapy resistance in cancer cells, and drugs that target store-independent Ca^{2+} entry pathways may have therapeutic potential in treating cancer.

1. Introduction

Ionized Ca^{2+} is a versatile, essential and ubiquitous second messenger that impacts all aspects of cell fate and function [1,2]. Free Ca^{2+} levels must be tightly regulated not only in the cytoplasm but also within individual organelles including the endoplasmic reticulum and secretory vesicles, components of the endo-lysosomal pathway, and mitochondria. Cross talk between the extracellular space, cytoplasm and individual organelles results in spatial and temporal modeling of Ca^{2+} signals [3] that decode intracellular (reactive oxygen species) and environmental (growth factors, hormones) cues to activate many downstream effector pathways integral to gene transcription, cell cycle control, differentiation, proliferation, cell migration, drug resistance and apoptosis [2,4,5]. Each of these Ca^{2+}-regulated processes is implicated in tumorigenesis [6–9]. Indeed, breast microcalcifications, which are dense deposits of mineralized calcium prominently visible in mammograms, are early warning signs of Ca^{2+} dysregulation that could lead to malignant tumors [10,11]. Understanding mechanisms of Ca^{2+} dysregulation could offer new insight into tumorigenesis and opportunities for therapeutic targeting.

One hallmark of tumorigenesis is the loss of mitochondrial Ca^{2+} homeostasis. Mitochondria have emerged as key players in the control of cell fate [12]. On the one hand, Ca^{2+} entry into mitochondria stimulates ATP production by oxidative phosphorylation and is a pro-survival signal. On the other hand, excessive mitochondrial Ca^{2+} triggers the apoptotic cascade leading to cell death. In recent years, some of the

Abbreviations: ER, estrogen receptor; PR, progesterone receptor; ROS, reactive oxygen species; SICE, store independent Ca^{2+} entry; SOCE, store operated Ca^{2+} entry; TNBC, triple negative breast cancer; TUNEL, Terminal deoxynucleotidyl transferase dUTP nick end labeling.

* Corresponding author. Department of Physiology, The Johns Hopkins University School of Medicine, 725 N. Wolfe Street Baltimore, MD, 21205, USA.
E-mail address: rrao@jhmi.edu (R. Rao).

https://doi.org/10.1016/j.redox.2022.102240
Received 2 November 2021; Received in revised form 11 January 2022; Accepted 14 January 2022
Available online 17 January 2022

molecular machinery involved in mitochondrial Ca^{2+} entry has been described [13]. The close proximity with endoplasmic reticulum Ca^{2+} stores and the formation of ER-mitochondrial membrane junctions results in microdomains of high Ca^{2+} concentrations that are believed to activate the low affinity mitochondrial Ca^{2+} uniporter (MCU) complex. Upon depletion of ER Ca^{2+} stores, ER sensors (STIM1,2) activate Orai1 or TRP Ca^{2+} channels on the plasma membrane by a mechanism known as store-operated Ca^{2+} entry (SOCE), to refill the ER and ensure subsequent refueling of mitochondrial Ca^{2+} stores. Surprisingly, evidence for direct coupling of mitochondrial Ca^{2+} entry to SOCE is scarce [14,15] suggesting that other mechanisms of mitochondrial Ca^{2+} entry may operate in the vicinity of the plasma membrane. This study reveals unexpected cross talk between mitochondria, plasma membrane and the secretory pathway that is important for mitochondrial Ca^{2+} entry and respiration.

The secretory pathway Ca^{2+}-ATPase SPCA2 (gene name *ATP2C2*) is highly expressed in the membranes of the Golgi and post-Golgi vesicles of secretory tissues such as the mammary epithelium [16–19]. SPCA2 plays an unusual dual role in Ca^{2+} homeostasis: in addition to its ATPase-dependent activity required for sequestering Ca^{2+} and Mn^{2+} ions into Golgi and vesicular stores, SPCA2 moonlights as a chaperone and activator of the Orai1 channel through interactions of its N- and C-terminal domains, to elicit robust Ca^{2+} influx at the plasma membrane [16,20–22]. This constitutive mechanism of Orai1 activation is termed store independent Ca^{2+} entry (SICE) [23] to distinguish it from SOCE, which is induced only upon depletion of endoplasmic reticulum Ca^{2+} stores. The pathophysiological roles of SICE are poorly understood. During lactation, upregulation of SICE may ensure efficient transepithelial basal to apical Ca^{2+} flux for the accumulation of 40–80 mM calcium in milk to nourish the newborn [24]. However, constitutively

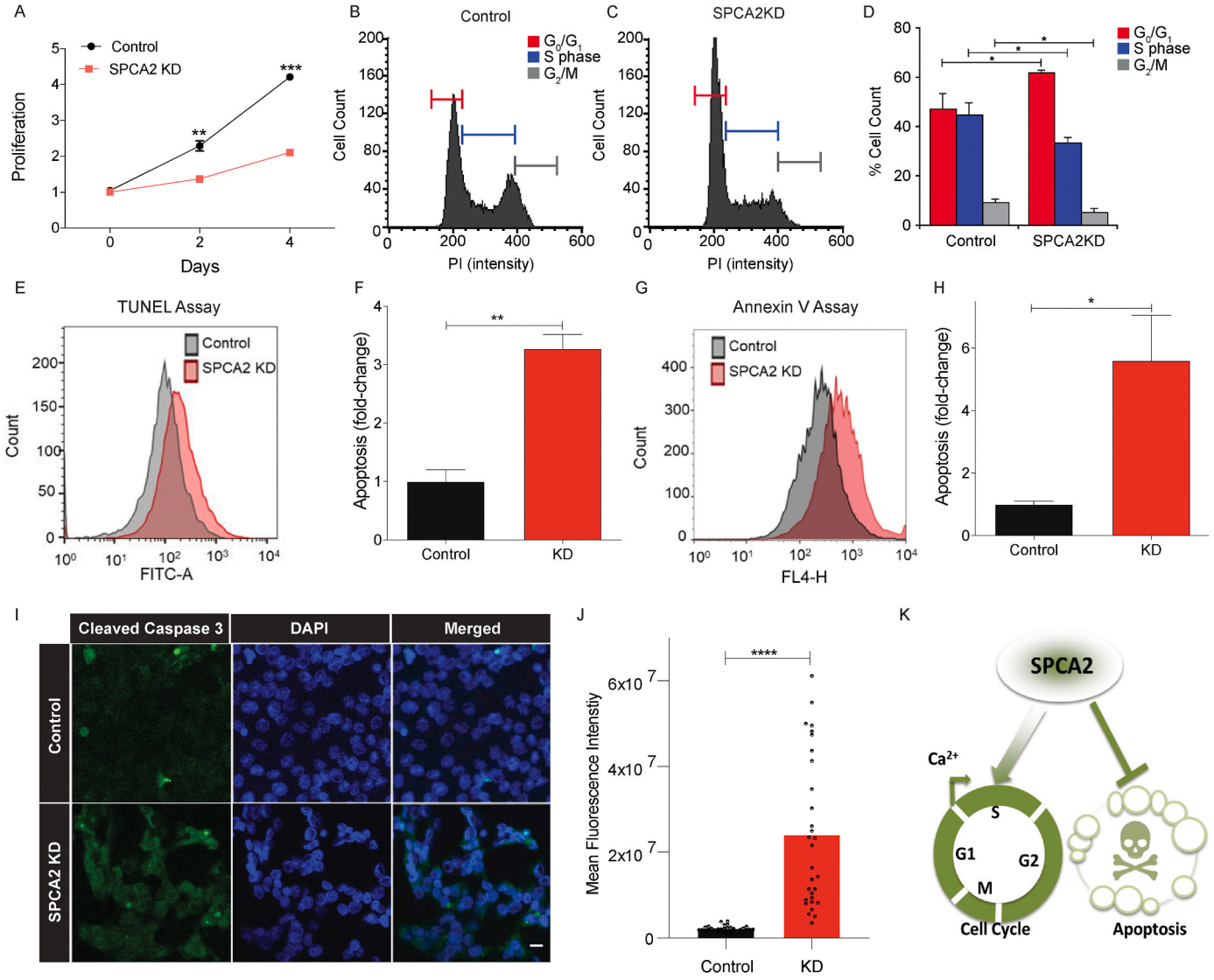

Fig. 1. SPCA2 drives cell cycle progression and survival. (A) Cell proliferation in MCF-7 is significantly decreased in SPCA2 KD compared to control, n = 3. (B–C) Representative cell cycle distribution (measured by propidium iodide staining) from flow cytometry of control and SPCA2 KD in MCF-7 cells. (D) SPCA2 KD increased percentage of cells in G_o/G_1 and correspondingly decreased S and G_2/M phase cells compared to control, n = 3. (E) Representative flow cytometry images showing apoptosis (measured by TUNEL staining) of control and SPCA2 KD in MCF-7 cells. (F) SPCA2 KD cells significantly increased apoptosis compared to control, n = 3. (G) Representative flow cytometry images showing apoptosis (measured by Annexin V fluorescence) of control and SPCA2 KD in MCF-7 cells. (H) SPCA2 KD cells significantly increased apoptosis compared to control, n = 3. (I) Representative confocal microscope images showing immunofluorescence staining of cleaved caspase-3 (marker for apoptosis) in MCF-7 control and SPCA2 KD cells (40× magnification; scale bar, 20 μm). (J) Fluorescence intensity of cleaved caspase-3 labeling was quantified by ImageJ software. SPCA2 KD showed significant increase in cleaved caspase-3 compared to control, n = 30 cells. (K) Schematic summarizing data showing that SPCA2 promotes cell cycle proliferation and blocks apoptosis. Significance: $^*P < 0.05$, $^{**}P < 0.01$, $^{***}P < 0.001$, $^{****}P < 0.0001$.

high expression of SPCA2 in hormone receptor positive breast cancers elevates SICE and activates the tumorigenic MAPK pathway [20]. We showed that silencing SPCA2 expression in ER+/PR+ murine xenograft models attenuated tumor formation *in vitro* and *in vivo* [20,25].

In this study, we describe a new role for SICE in maintaining genomic integrity, controlling ROS production and mitochondrial respiration. In the absence of SPCA2, or brief depletion of extracellular Ca^{2+} to block SICE, single and double stranded DNA breaks appeared, activating the ATM/ATR-p53 DNA damage response pathway. We uncover an unexpected link between SICE, mitochondrial Ca^{2+} entry and mitochondrial respiration that is critical for protection against ROS-mediated DNA damage. One therapeutic implication is that elevated levels of SPCA2 confer cancer cell resistance to DNA damaging agents, including carboplatin, doxorubicin and ionizing radiation. In summary, we describe novel pump-independent functions of SPCA2 that have far reaching cellular consequences for mitochondrial function, redox homeostasis, and DNA damage response.

2. Results

2.1. SPCA2 promotes cell cycle progression and survival by activating store-independent Ca^{2+} entry

High levels of SPCA2 have been associated with increased cell proliferation [20,25]. To understand why, we used a breast cancer cell model MCF-7 that expresses high endogenous SPCA2 [25]. Knockdown of SPCA2 in MCF-7 (Fig. S1A) significantly reduced cell growth determined by colorimetric assay of viable cells (Fig. 1A) and BrdU incorporation (Fig. S1B). Cell cycle analysis revealed an accumulation of SPCA2 KD cells in the G0/G1 phase, which increased from about 40% in control to 60%, and a concomitant decrease in the number of cells that progressed to the S and G2/M phases (Fig. 1B–D). The ability of SPCA2 to drive proliferation was confirmed in multiple cell lines and was independent of estrogen receptor or tumor status: SPCA2 KD inhibited cell growth in the receptor negative, non-cancerous MCF10-A cell line (Figs. S1C–D), and in the receptor positive ZR-75 breast cancer line (Figs. S1E–F). Furthermore, ectopic expression of SPCA2 in triple receptor negative breast cancer cell lines Hs578T (Fig. S1G) and MDA-MB-231 (ahead, Fig. 2D) with low endogenous SPCA2 [25] substantively increased cell proliferation.

One outcome of cell cycle arrest is apoptosis [26]. Hallmarks of apoptosis increased in MCF-7 following knockdown of SPCA2, as evidenced by PI and TUNEL staining (Fig. 1E and F; Fig. S1H), externalization of phosphatidylserine (Fig. 1G and H) and staining for cleaved caspase-3 (Fig. 1I and J). We conclude that SPCA2 plays a proliferative and pro-survival role in these cells (Fig. 1K).

The ability of SPCA2 to drive cell proliferation could be due to accumulation of Ca^{2+} in secretory pathway stores where it is important

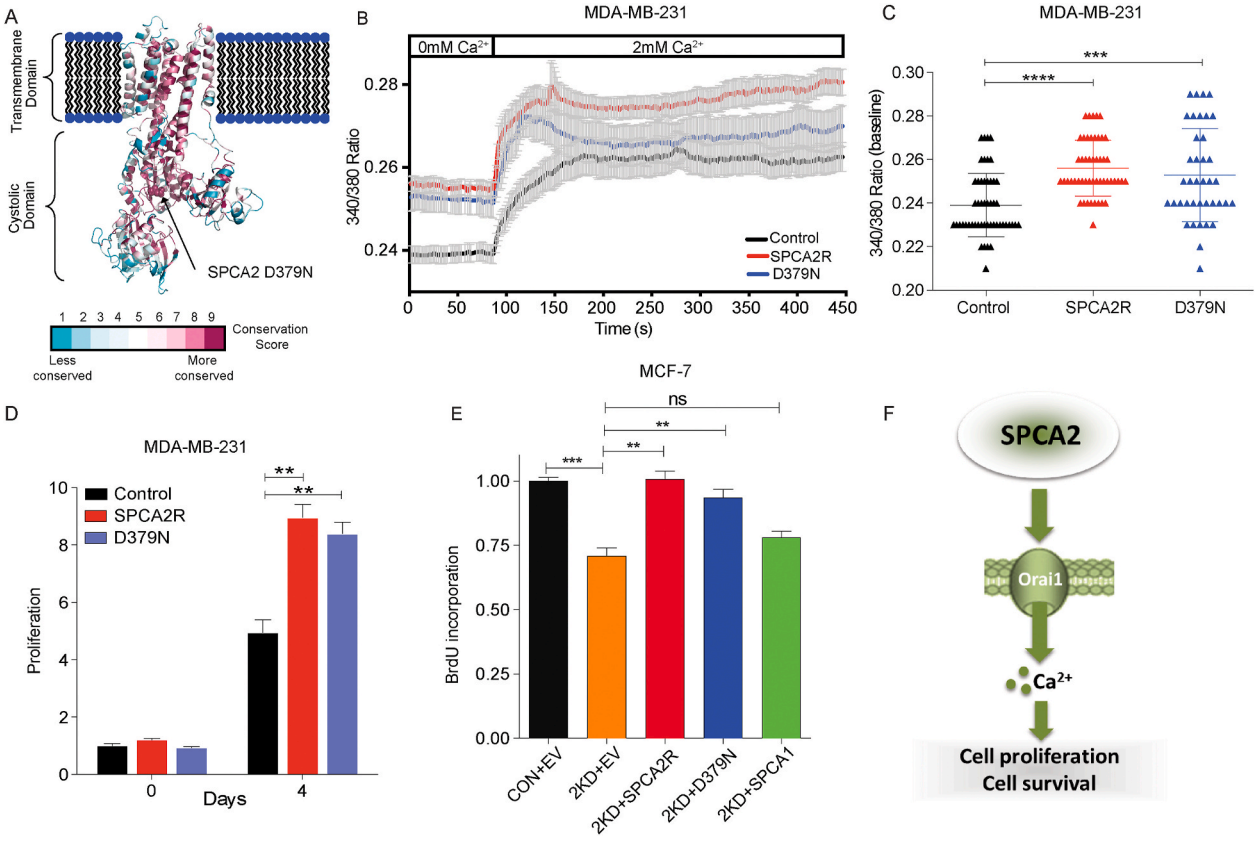

Fig. 2. ATPase deficient mutation in SPCA2 does not block cell proliferation or Ca^{2+} entry. (A) Schematic of SPCA2 loss of function mutation D379N, located in the highly conserved phosphorylation domain essential for transport activity in all P-type ATPases. (B) Live cell Ca^{2+} imaging traces of Fura2-AM treated MDA-MB-231 cells with or without SPCA2R and SPCA2 D379N (Control n = 51 cells, SPCA2R n = 50 cells, SPCA2 D379N n = 39). Baseline readings in Ca^{2+}-free conditions were established for 80 s and then cells were recorded under 2 mM Ca^{2+} conditions for 6 min and 20 s. (C) Baseline Ca^{2+} levels (340/380 nm ratio of Fura-2 fluorescence) are significantly increased in cells overexpressing SPCA2 and SPCA2 D379N in MDA-MD-231 compared to vector control. Control n = 51 cells, SPCA2R n = 50 cells, SPCA2 D379N n = 39. (D) Ectopic expression of SPCA2 and SPCA2 D379 N in MDA-MB-231 increased cell proliferation compared to control, n = 3. (E) Silencing resistant recombinant SPCA2 or ATPase-deficient mutant (SPCA2R, D379 N) constructs significantly restore BrdU incorporation defect in MCF-7 SPCA2 KD cells, relative to SPCA2 KD cells (2KD) transfected with empty vector (EV). SPCA1 does not significantly restore BrdU incorporation levels to SPCA2 KD cells, n = 5 for control, n = 3 for other groups. (F) Schematic showing that SPCA2 activates Ca^{2+} influx through Orai1 channels to increase cell proliferation and survival. Significance: $^{ns}P > 0.05$, $^{*}P < 0.05$, $^{**}P < 0.01$, $^{***}P < 0.001$, $^{****}P < 0.0001$.

for processing and secretion of proteins [27]. However, ectopic expression of the functionally related Ca^{2+}-ATPase isoform, SPCA1 [28] did not increase cell proliferation of MCF-7 cells (Figs. S2A–B). In contrast, even though SPCA2 was already highly expressed in MCF-7 [10,25], ectopic expression of SPCA2 conferred further significant, albeit modest increase in cell proliferation (Figs. S2C–D). Furthermore, the cell proliferation phenotype observed for SPCA2 knockdown could be rescued by a silencing-resistant construct, SPCA2R, but not by SPCA1 (Figs. 2E and S2E, G-H). The isoform-specificity of these observations suggest that luminal Golgi Ca^{2+} is not critical for proliferation, and that SPCA2 may be driving cell growth by a pump-independent mechanism.

Previously, we showed that SPCA2 activates plasma membrane Orai1 channels to elicit Ca^{2+} influx through an isoform-selective, pumping-independent mechanism known as store-independent Ca^{2+} entry, SICE [20]. Using Fura-2 fluorescence as Ca^{2+} indicator, we showed that SPCA2 KD in MCF-7 cells lowers resting Ca^{2+} levels and diminishes store-independent Ca^{2+} entry through Orai1 [20]. To test the possibility that SICE mediates cell proliferation effects described here, we used the previously characterized loss of function mutation D379N [10,29]. Located in the highly conserved phosphorylation domain, this aspartic acid residue is essential for transport activity in all P-type ATPases (Fig. 2A). We show that expression of mutant D379N in MDA-MB-231 cells which have low endogenous SPCA2 levels [25,29] can elicit Ca^{2+} entry (Fig. 2B), to elevate basal Ca^{2+} levels (Fig. 2C), similar to wild type SPCA2 [25,29]. Expression of mutant D379 N also increased cell proliferation in MDA-MB-231 cells, similar to wild type SPCA2 (Fig. 2D) and rescued cell proliferation defects of SPCA2 KD in MCF-7 (Figs. 2E and S2F) suggesting a link between cell proliferation phenotypes and SICE. Previously published observations also showed that depletion of external Ca^{2+} significantly reduces the G1 phase Cyclin D protein [30] and that Orai1 silencing inhibits cell proliferation and causes G1 arrest [31]. Here, we confirm that blocking Ca^{2+} entry with the inhibitor SKF-96365 [32] phenocopies the cell proliferation and viability defects of SPCA2 knockdown (Figs. S2I–J). Taken together, these data suggest that the ability of SPCA2 to activate store-independent Ca^{2+} entry (SICE) and increase baseline cytoplasmic

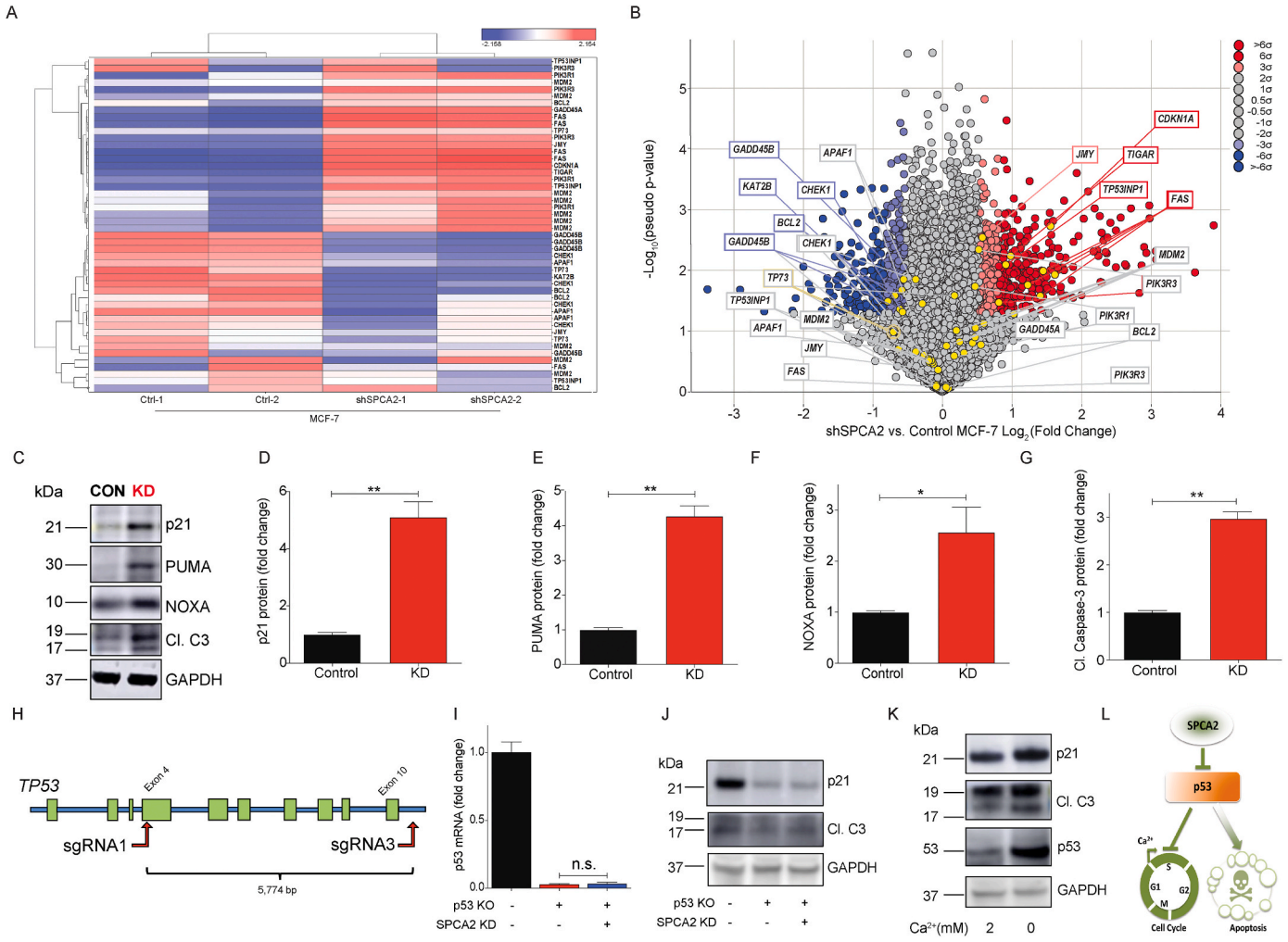

Fig. 3. Loss of SPCA2 activates the p53 pathway. (A) Heat map with dendrogram indicating differential expression of p53 pathway genes identified from Ingenuity Pathway Analysis. Multiples relate to individual probe sets from the Affymetrix Human Genome U133 Plus 2.0 Array. (B) Volcano plot calculated using pseudo *P* values calculated by one-way ANOVA versus the Log_2 (fold change). Several p53 pathway genes, indicated in boxes, are highly up (red box) or down regulated (blue box). Color shading correlates with significance of change. (C) Representative western blotting images of p21, PUMA, NOXA, and cleaved caspase-3 in MCF-7 control and SPCA2 KD cells, with GAPDH used as a loading control. (D–G) SPCA2 KD in MCF-7 showed a significant increase in protein level of p53 downstream effector molecules p21, PUMA, NOXA, and cleaved caspase-3 compared to control, n = 3. (H) Schematic showing strategy for generating *TP53* gene KO in MCF-7 cells. (I) p53 transcript was not detected in the *TP53* KO MCF-7 cells. (J) SPCA2 KD did not increase p21 and cleaved caspase-3 in *TP53* KO MCF-7 cell line. (K) Brief exposure (2 h) of MCF-7 cells to Ca^{2+}-free medium increased expression of p53 and its downstream effectors p21 and cleaved caspase, relative to standard (2 mM Ca^{2+}) medium. (L) Schematic showing SPCA2 promotes cell cycle proliferation and blocks apoptosis via p53 pathway. Significance: $^{ns}P > 0.05$, $^{*}P < 0.05$, $^{**}P < 0.01$, $^{***}P < 0.001$. (For interpretation of the references to color in this figure legend, the reader is referred to the Web version of this article.)

Ca^{2+} may drive cell cycle progression at the G1/S checkpoint and cell survival (Fig. 2F).

2.2. Store-independent Ca^{2+} entry inhibits p53 signaling

As a starting point to understand the signaling mechanisms linking SPCA2 to cell growth and survival, we analyzed the effect of SPCA2 KD on the transcriptome of MCF-7 cells. Consistent with our observations in Fig. 1, top molecular and cellular function categories altered, relative to control, were Cell Death and Survival (P value range of 2.44E-06 – 1.00E-22), and Cell Growth and Proliferation (P value range of 2.53E-06 – 3.80E-15), with 467 and 495 differentially expressed genes identified, respectively. Among the top canonical pathways identified by Ingenuity analysis, p53 signaling was significantly up regulated ($P = 3.87E-04$) in SPCA2 KD cells (Fig. 3A and B). We confirmed mRNA alterations in a representative set of p53 pathway genes by qPCR analysis (Table S1).

Activation of p53 is critical for G0/G1 cell cycle checkpoint arrest by inducing expression of the cyclin-dependent kinase inhibitor p21, and for apoptosis by transcriptional activation of the pro-apoptotic Bcl-2 family members PUMA and NOXA [33]. Western blot analysis showed that protein levels of p21, PUMA, and NOXA in MCF-7 SPCA2 KD were significantly increased compared to control (Fig. 3C–F). Pro-apoptotic proteins activate serine protease caspases, leading to apoptosis [34]. There was a significant increase in cleavage of caspase-3 in SPCA2 KD compared to control (Fig. 3C and G). Similar results were observed following SPCA2 KD in the ZR-75 cell line (Figs. S3A–B). In contrast, KD of the housekeeping isoform SPCA1 in MCF-7 did not increase cell cycle or apoptosis markers (Figs. S3C–D). To confirm the critical role of p53 in mediating pro-survival phenotypes in SPCA2 KD, we engineered a stable knockout of the *TP53* gene in MCF-7 (Fig. 3H and I) and generated SPCA2 KD in this cell line (Fig. S3E). In the absence of p53, there was no increase in protein levels of p21 or cleaved caspase-3 following SPCA2 KD (Fig. 3J), and no increase in transcript levels of p21, PUMA or NOXA (Fig. S3 F–H).

Since Orai1 is a major downstream effector of SPCA2 in mediating SICE in breast cancer cells [30], we predicted that loss of Orai1 activity would phenocopy loss of SPCA2. Here we show that knockdown (Figs. S3I–K) or inhibition of Orai1 with SKF-96365 [32] (Fig. S3L-M) in MCF7 also induces expression of p21 and NOXA mRNA. Brief (2 h) removal of external Ca^{2+} from the culture medium, by chelation with EGTA, was sufficient to increase p53 levels, and concomitantly increase p21 and cleaved caspase-3 (Fig. 3K). We conclude that store-independent Ca^{2+} entry inhibits p53 to mediate the proliferative and pro-survival effect of SPCA2 (Fig. 3L).

2.3. Store-independent Ca^{2+} entry protects against DNA damage

Activation of p53 is mediated mainly through uncoupling from its key negative regulator MDM2, following phosphorylation by the serine/threonine protein kinases ATM/ATR in response to DNA damage [35]. Therefore, we investigated a potential link between loss of SPCA2 and DNA damage. There was a significant increase ($P < 0.001$) in nuclear staining and expression of the double-stranded DNA damage marker p-H2AX (Fig. 4A–C), as well as the single-stranded DNA damage marker F7-26 ($P < 0.001$) (Fig. 4D and E) in SPCA2 KD cells compared to control. Downstream effectors in the DNA damage response pathway were activated in SPCA2 KD cells, as evidenced by the increase ($P < 0.05$) in phosphorylation of ATM, ATR, and p53 (Fig. 4F–I). Comparable results were observed upon SPCA2 KD in MCF-10A (Figs. S4A–B). Similar to their effect on cell proliferation (Fig. 2E), both SPCA2R and SPCA2 D379N reversed the observed increase of p-H2AX in MCF-7 SPCA2 KD cells, as compared to the empty vector control (Fig. 4J). As expected, there was no difference in protein levels of downstream molecular markers of DNA damage, cell cycle arrest or apoptosis between control MCF-7 cells and SPCA2 KD cells rescued with SPCA2R or D379N constructs (Figs. S4C–E). In contrast, SPCA1 was unable to reverse increased levels of cell cycle arrest marker p21 (Fig. S4F) and apoptosis marker NOXA (Fig. S4G) seen in SPCA2 KD cells. Further, there remained a significant increase in DNA damage marker p-H2AX in SPCA1 expressing cells compared to control (Figs. S4H and I). Therefore, we conclude ectopic expression of SPCA1 cannot rescue SPCA2 KD.

Next, we asked if extracellular Ca^{2+} played a role in SPCA2-mediated DNA damage response. We show that a brief (1 h) exposure of MCF-7 cells to Ca^{2+}-free medium increased phosphorylation of H2AX and p53 (Fig. 4K). These findings reveal an unexpected and novel role for SPCA2-mediated extracellular Ca^{2+} entry in maintaining genomic integrity and regulating the DNA damage response (Fig. 4L).

2.4. Loss of SPCA2 expression sensitizes cells to DNA damaging agents

Drugs that elicit the DNA damage response, including carboplatin, doxorubicin and ionizing radiation, are used as neoadjuvant therapy for breast cancer patients [36,37]. Since SPCA2 KD increased DNA damage and activation of ATM/ATR-p53 pathway, we hypothesized that loss of SPCA2 expression would sensitize breast cancer cells to DNA damaging agents. We show that MCF-7 SPCA2 KD cells are more sensitive to carboplatin, doxorubicin and ionizing radiation, compared to control (Fig. 5A–C). Similarly, SPCA2 KD conferred doxorubicin sensitivity to non-cancer MCF-10A cells (Fig. S5A). As expected, cell survival differences in doxorubicin were abolished following the rescue of knockdown using SPCA2R (Fig. 5D). Further increase in SPCA2 expression in MCF-7 (SPCA2R; Fig. S2C) was found to significantly blunt ($P < 0.01$) doxorubicin cytotoxicity (Fig. S5B). Even in the low endogenous SPCA2 expressing cell line MDA-MB-231, treatment with doxorubicin significantly increased DNA damage in SPCA2 KD cells [29] compared to control (Figs. S5C and D).

Since removal of extracellular Ca^{2+} or knockdown of SPCA2 increased DNA damage, leading to increased sensitivity to DNA damaging agents, we asked if doxorubicin cytotoxicity was modulated by extracellular calcium. We show that culturing MCF-7 cells in increasing concentrations of calcium significantly rescued doxorubicin cytotoxicity ($P < 0.05$) (Fig. 5E and F). We conclude that SPCA2 mediates a novel chemoresistance mechanism that links Ca^{2+} homeostasis to the response to DNA damaging chemotherapeutic drugs (Fig. 5G).

2.5. Store independent Ca^{2+} entry inhibits mitochondrial ROS production

Intracellular reactive oxygen species (ROS) are known to initiate DNA damage and activate the ATM/ATR-p53 pathway [38]. Therefore, we evaluated the effect of SPCA2 on ROS production. SPCA2 KD significantly increased ($P < 0.001$) endogenous levels of ROS, as measured by DCFDA fluorescence, in MCF-7 (Fig. 6A and B) and MCF-10A (Figs. S6A–B). In response to oxidative stress induced by treatment with H_2O_2, ROS levels were further elevated, with SPCA2 KD cells showing greater increase ($P < 0.05$) compared to control (Fig. 6A–B, **S6A-B**). Similarly, brief removal (10 min) of extracellular Ca^{2+} significantly increased ROS compared to cells maintained in 2 mM calcium, and the absence of Ca^{2+} exacerbated ROS production in the presence of H_2O_2 (Fig. 6C and D). In MCF-7, there was no difference in ROS production between control cells and SPCA2 KD cells following rescue with silencing-resistant SPCA2R construct, both in the absence or presence of H_2O_2 (Figs. S6C–D).

Mitochondria are one the principle generators of ROS, through activity of the electron transport chain [39]. We observed a significant increase ($P < 0.05$) of mitochondrial ROS (MitoSOX-Red) in SPCA2 KD compared to control (Fig. 6E and F). Doxorubicin was previously reported to induce mitochondrial ROS [40]. Upon doxorubicin treatment, there was significantly more ($P < 0.01$) mitochondrial ROS generation in SPCA2 KD compared to control (Fig. 6E and F).

We asked if addition of anti-oxidants (N-acetyl cysteine + vitamin C) known to block ROS [41–44], rescue the activation of DNA damage response in SPCA2 KD cells. We found that anti-oxidants decrease

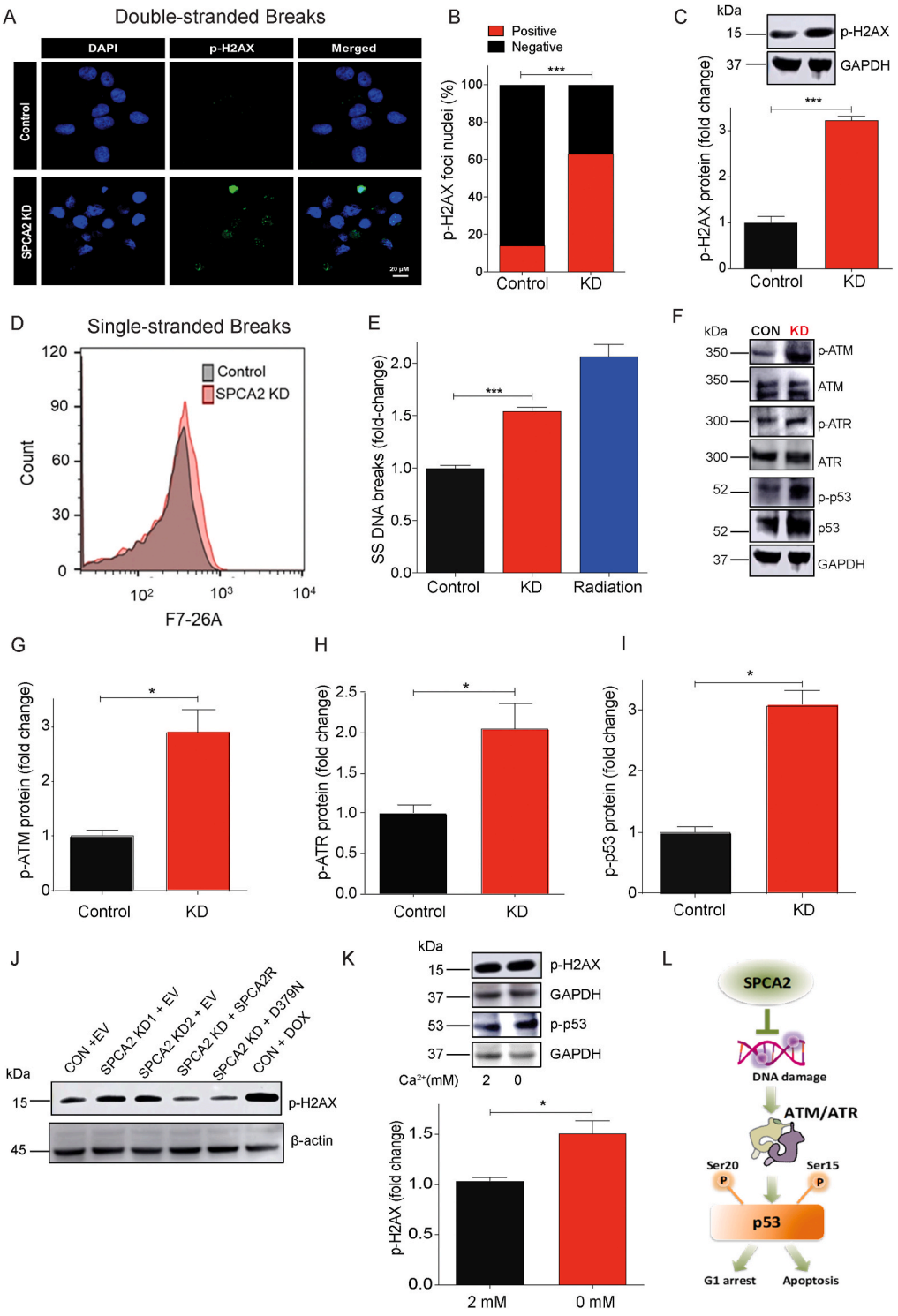

Fig. 4. Loss of SPCA2 activates DNA damage and ATM/ATR-p53 pathway. (A) Representative confocal microscope images showing immunofluorescence staining of p-H2AX (marker for double stranded DNA breaks) in MCF-7 control and SPCA2 KD cells (40× magnification; scale bar, 20 μm). (B) p-H2AX positive and negative nuclei are quantified by ImageJ software. SPCA2 KD showed significant number of p-H2AX positive nuclei compared to control. n = 247 in control, n = 250 for SPCA2 KD. (C) p-H2AX protein expression was detected using western blotting; GAPDH was used as a loading control. SPCA2 KD significantly increased p-H2AX expression compared to control, n = 3. (D) Representative flow cytometry images showing F7-26 staining (marker for single stranded DNA breaks DNA breaks) in MCF-7 control and SPCA2 KD cells. (E) Single stranded DNA breaks are significantly higher in SPCA2 KD compared to control. Radiation treatment (10 Gy) was used as positive control, n = 3. (F) Representative western blotting images of ATM, p-ATM, ATR, p-ATR, p53, and p-p53 in MCF-7 control and SPCA2 KD cells; GAPDH was used as a loading control. (G–I) Densitometry of western blots shows SPCA2 KD significantly increased p-ATM, p-ATR, p-p53 compared to control, n = 3. (J) Representative western blotting image of p-H2AX in MCF-7 control + Empty vector (EV), SPCA2 KD + EV, SPCA2 rescued cells (KD + SPCA2R, and KD + D379N), control + DOX (doxorubicin, DOX, 250 nM, 24 h, used as positive control); β-actin was used as a loading control. (K) MCF-7 cells were exposed to calcium free media (0 mM) for 1 h, and cell lysates examined by western blotting. p-H2AX and p-p53 increased relative to cells grown in media with 2 mM calcium. Densitometric analysis shows increased p-H2AX in cells exposed to Ca^{2+} free medium, n = 3. (L) Schematic showing SPCA2 blocks DNA damage and downstream activation of ATM/ATR-p53 pathway leading to cell cycle arrest and apoptosis. Significance: $^{*}P < 0.05$, $^{***}P < 0.001$.

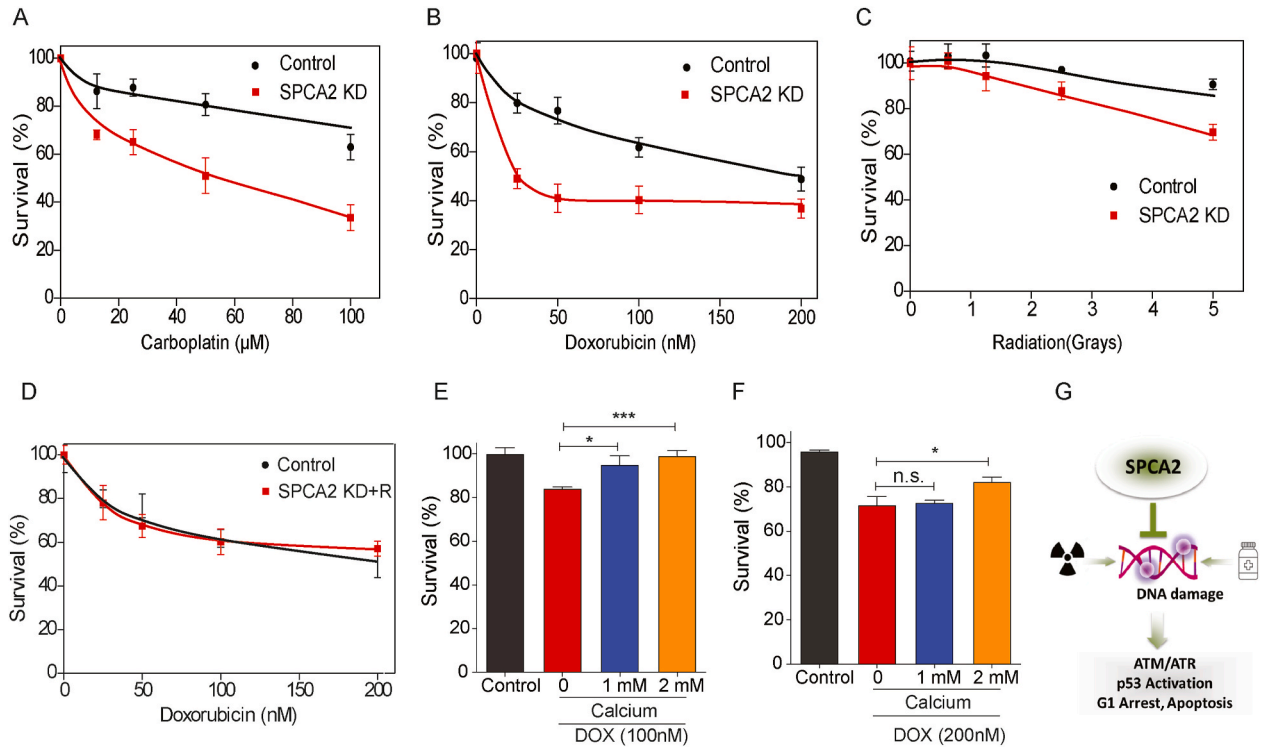

Fig. 5. Loss of SPCA2 expression sensitizes cells to DNA damaging agents. (A-C) Dose-response curves of control and SPCA2 KD in MCF-7 cells. Error bars represent standard deviation (n = 5 or 6). Approximately 3 000–5000 cells were seeded into 96 well plates, and incubated overnight. Cells were treated with drugs 120 h before MTT cytotoxicity analysis. The survival fraction was determined by mean fluorescence of the treated cells/mean fluorescence of control cells, and normalized to untreated. SPCA2 KD increased chemosensitivity to the DNA damaging agents doxorubicin (0–200 nM), carboplatin (0–100 μM), and radiation (0–5 Gy). (D) SPCA2 KD rescued cells in MCF-7 cells did not increase chemosensitivity to doxorubicin (0–200 nM) compared to control (n = 5 or 6, time = 120 h). (E–F) Approximately 10,000 cells were seeded into 96 well plates in Ca^{2+}-free media supplemented with 2% FBS without addition of EGTA, and incubated overnight. Cells were treated with doxorubicin (100 and 200 nM) for 48 h, along with/without addition of Ca^{2+} (1 mM and 2 mM). Cells cultured in Ca^{2+}-free media were considered as control. Culturing MCF-7 cells with increasing concentration of Ca^{2+} significantly rescued doxorubicin cytotoxicity. n = 5 for 100 nM, n = 4 for 200 nM. (G) Schematic showing Loss of SPCA2 expression sensitizes cells to DNA damaging agents. Significance: $^{ns}P > 0.05$, $^{*}P < 0.05$, $^{***}P < 0.001$.

activation of the ATM/ATR-p53 mediated pathway, as seen by decrease in phosphorylated ATR, p53 and p21, increased expression of Cyclin D1, decreased production of cleaved caspase-3 and decreased levels of p-H2AX in SPCA2 KD cells (Fig. 6G, S6E-J). Taking into account the concentration of anti-oxidants used and time period administered, the potency of anti-oxidants is not likely to be 100%. Nevertheless, we now show that addition of N-acetyl cysteine alone significantly rescued cell proliferation, as determined by incorporation rates of BrdU (Fig. S6K). Similarly, addition of mitochondrial-specific antioxidant Mito-TEMPO to SPCA2 KD reduced cleaved caspase 3, p21 expression and p-H2AX levels in MCF-7 KD cells (Fig. 6H, S6L-N).

The electron transport chain is the primary source of mitochondrial ROS, in the form of superoxide radicals that are converted to H_2O_2 as a first step in detoxification by the mitochondrial-specific manganese superoxide dismutase (MnSOD/SOD2) [45]. We observed a significant decrease in expression of SOD2 in SPCA2 KD cells compared to control (Fig. 6I), suggesting a disruption of ROS scavenging mechanisms in mitochondria that could account, at least in part, for increased ROS in SPCA2 KD cells. Taken together, our results reveal a novel role for SPCA2 and store-independent Ca^{2+} entry to protect against ROS, DNA damage and activation of ATM/ATR-p53 pathways (Fig. 6J).

2.6. *Store-independent Ca^{2+} entry is required for mitochondrial respiration*

Regulated Ca^{2+} uptake into mitochondria is essential for the activity of several mitochondrial enzymes that are required for maintenance of the mitochondrial membrane potential and ATP generation by oxidative phosphorylation [46]. Mechanisms of mitochondrial Ca^{2+} transfer through ER junctional contacts have been described, and these require STIM-Orai interactions and activation of store-operated Ca^{2+} entry to replenish ER stores. We used the mitochondrial Ca^{2+} sensor Rhodamine 2-AM [47] to assess the contribution of SPCA2 and SICE to mitochondrial Ca^{2+} levels. We observed a significant decrease in mitochondrial Ca^{2+} in SPCA2 KD cells compared to MCF-7 controls by confocal microscopy (Fig. 7A and B; $P < 0.05$), and flow cytometry (Fig. 7C and D; $P < 0.001$). Similar results were observed in non-tumor MCF-10A cell line (Figs. S7A–B). Brief (10 min) removal of extracellular Ca^{2+} significantly decreased ($P < 0.001$) mitochondrial calcium when compared to cells maintained in 2 mM calcium (Fig. 7E and F).

We hypothesized that defective mitochondrial Ca^{2+} entry in the absence of SPCA2 and SICE would lead to mitochondrial dysfunction, evidenced by depolarization of the mitochondrial membrane potential. We used the membrane-permeant JC-1 dye which exhibits potential-dependent accumulation and aggregation in mitochondria to evaluate membrane potential [48]. Thus, treatment of cells with the drug 4-HPR known to depolarize mitochondria [49,50] resulted in decreased mitochondrial accumulation (red) and increased cytoplasmic levels (green) of JC-1 monomers (Fig. 7G–H, Fig. S7C). We observed a significant increase ($P < 0.001$) in mitochondrial depolarization in SPCA2 KD cells compared to control (Fig. 7G and H), and the red to green ratio of JC-1 was significantly decreased in SPCA2 KD compared to control (Fig. S7C). Similarly, brief removal (10 min) of extracellular Ca^{2+} significantly increased ($P < 0.001$) mitochondrial depolarization compared to cells maintained in 2 mM calcium (Figs. S7D–E). We also compared expression of Tom20, an outer mitochondria membrane protein, in MCF-7 control and SPCA2 KD cells. The absence of significant changes in Tom20 expression suggest that there is no significant change in

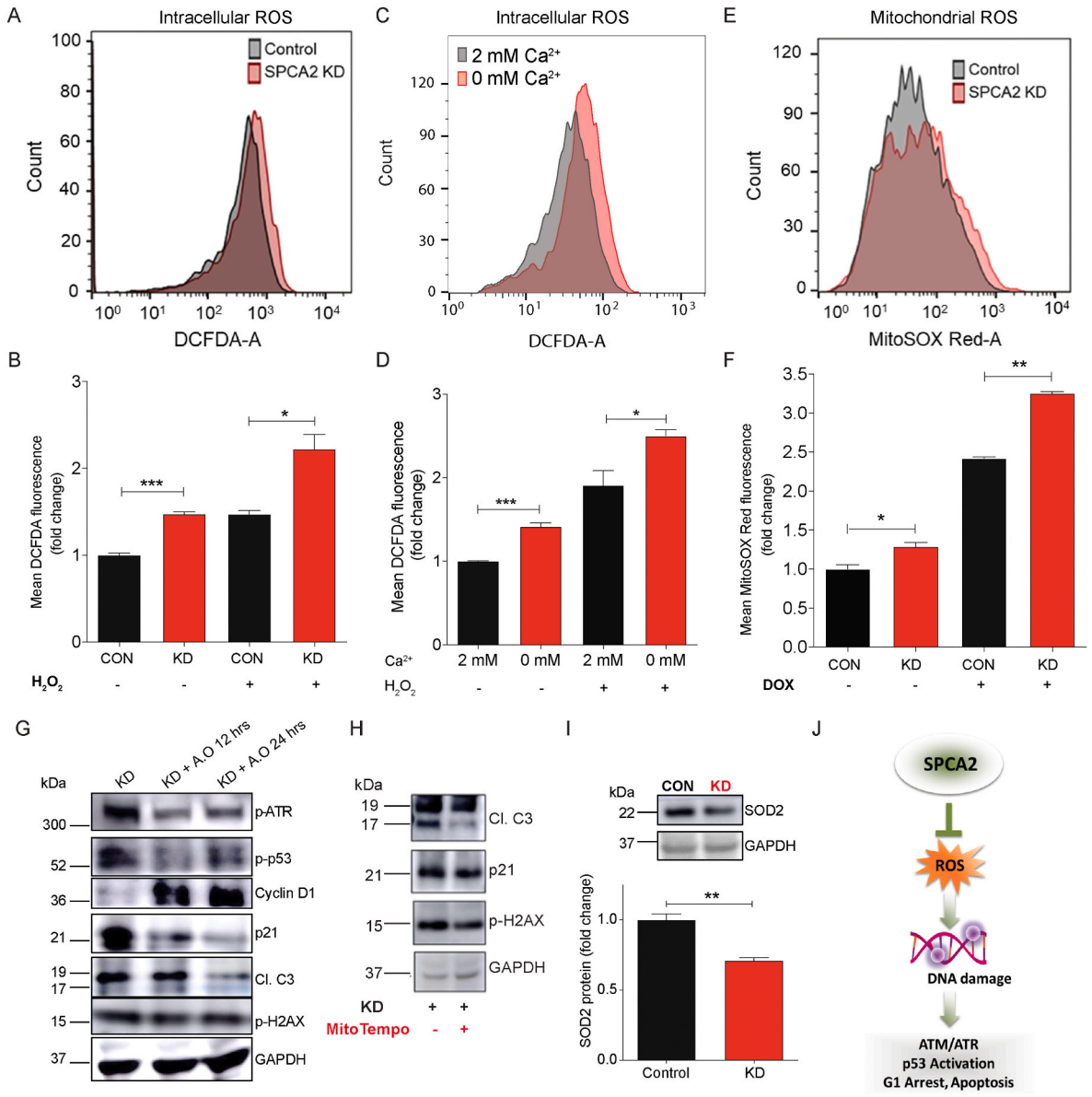

Fig. 6. SPCA2 protects against ROS-mediated DNA damage. (A) Representative flow cytometry images showing ROS (DCFDA fluorescence) in MCF-7 control and SPCA2 KD cells. (B) ROS production was significantly increased compared to control. H_2O_2 (500 μM for 20 min) was used as positive control; n = 6 for SPCA2 KD and control; n = 3 for H_2O_2 experiment. (C) Representative flow cytometry showing ROS (DCFDA) in MCF-7 cells exposed to Ca^{2+}-free media for 10 min compared to cells grown in media with 2 mM Ca^{2+}. (D) ROS production increased in Ca^{2+}-free media; H_2O_2 (500 μM for 15 min) was used as positive control, n = 3. (E) Representative flow cytometry showing mitochondrial ROS (MitoSOX-Red) of MCF-7 control and SPCA2 KD cells. (F) Mitochondrial ROS was significantly increased in SPCA2 KD compared to control. Doxorubicin was used as positive control (500 nM for 24 h), n = 3. (G) Anti-oxidants (Vitamin C, 500 μM + N-acetyl cysteine, 500 μM) were added to MCF-7 SPCA2 KD cells for 12 h and 24 h and immunoblotting is performed using GAPDH as loading control. Anti-oxidants decreased p-ATM, p-p53, p21, cleaved caspase-3, p-H2AX, and increased cyclin D1. (H) Mitochondrial anti-oxidant (MitoTempo, 5 μM) was added to MCF-7 SPCA2 KD cells for 24 h and immunoblotting was performed using GAPDH as loading control. MitoTempo decreased levels of cleaved caspase-3, p21, and p-H2AX. (I) SOD2 protein expression was detected using western blotting, and GAPDH was used as a loading control. SPCA2 KD significantly decreased SOD2 expression compared to control, n = 3. (J) Schematic showing SPCA2 blocks ROS mediated activation of DNA damage, activation of ATM/ATR-p53 pathway, resulting in cell cycle arrest and apoptosis. Significance: $^*P < 0.05$, $^{**}P < 0.01$, $^{***}P < 0.001$. . (For interpretation of the references to color in this figure legend, the reader is referred to the Web version of this article.)

mitochondrial mass in SPCA2 knockdown compared to control (Figs. S7F–G).

Mitochondrial membrane potential derives from cellular respiration, a process by which the electron transport chain consumes oxygen to produce ATP. Measurements of oxygen consumption rate revealed significantly ($P < 0.0001$) reduced rates of basal and maximal respiration, and lowered ATP production, in the absence of SPCA2 (Fig. 8A and B), mimicking the absence of extracellular Ca^{2+} (Fig. 8C and D. Non-mitochondrial respiration was unchanged (Fig. 8B, D). We conclude that SPCA2 mediated Ca^{2+} entry into mitochondria is required for cellular respiration and the generation of mitochondrial membrane potential.

In summary, we show that SPCA2 elicits Ca^{2+} influx through Orai1 channels at the plasma membrane, by a mechanism independent of ATP hydrolysis. Mitochondrial uptake of Ca^{2+} resulting from this SPCA2-mediated mechanism maintains mitochondrial respiration and membrane potential. In the absence of SPCA2, mitochondrial ROS causes single and double stranded breaks in DNA, activating the ATM/ATR-p53

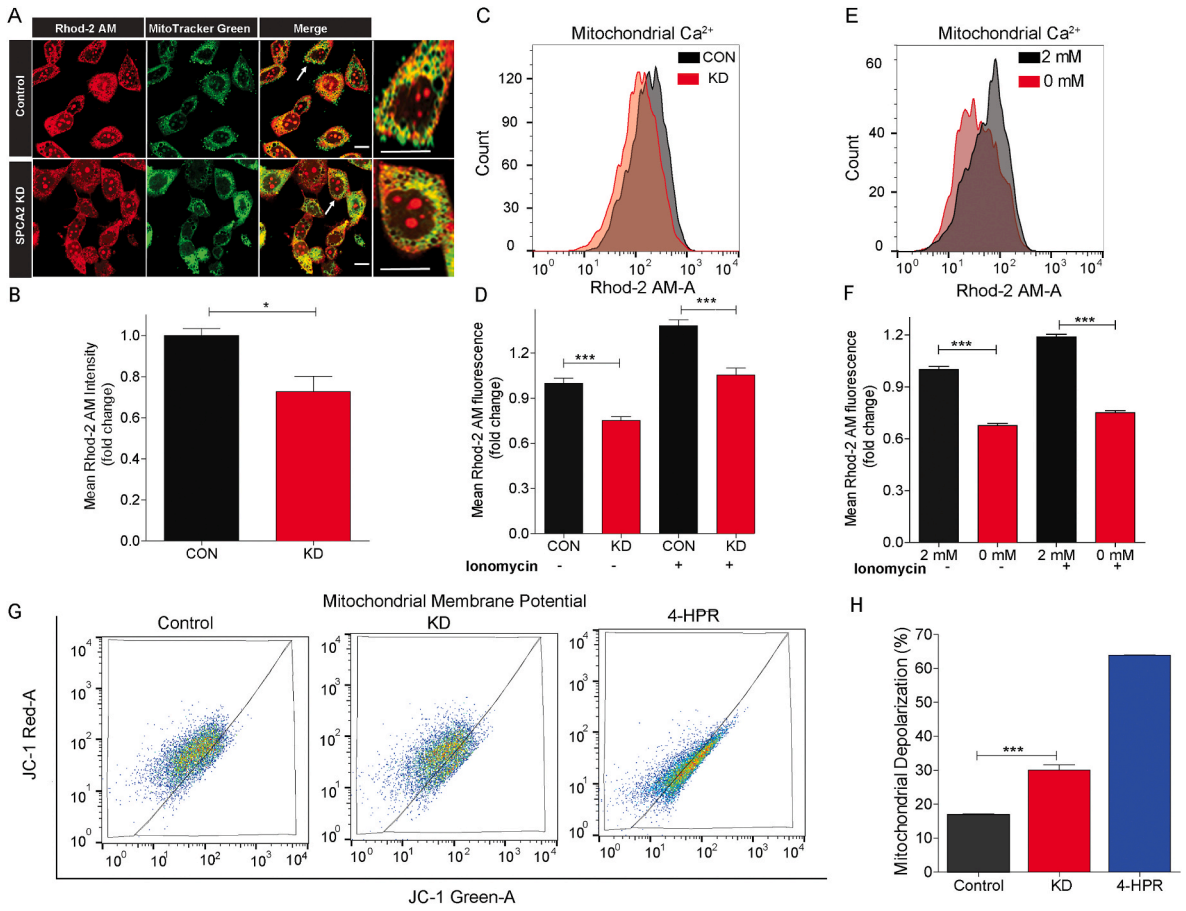

Fig. 7. SPCA2 regulates mitochondrial Ca^{2+} and membrane potential. (A) Representative confocal microscope images showing fluorescence of Rhod 2-AM (marker for mitochondrial calcium), MitoTracker Green (marker for mitochondria) in MCF-7 control and SPCA2 KD cells (scale bar, 10 μm). The cells indicated with the arrow are further enlarged to show co-localization. (B) Mean Rhod-2 AM intensity is quantified by ImageJ software. SPCA2 KD showed significantly lower mean Rhod-2 AM intensity compared to control. n = 36 in control, n = 57 for SPCA2 KD, from 7 images each. (C) Representative flow cytometry images showing mitochondrial calcium (Rhod-2 AM fluorescence) in MCF-7 control and SPCA2 KD cells. (B) Mitochondrial calcium was significantly decreased in SPCA2 knockdown compared to control. Ionomycin (10 μM for 15 s) was used as positive control; n = 6 for control and n = 4 for SPCA2 KD. (E) Representative flow cytometry showing mitochondrial calcium in MCF-7 cells exposed to Ca^{2+}-free media for 10 min compared to cells grown in media with 2 mM Ca^{2+}. (F) Mitochondrial calcium decreased in MCF-7 cells exposed to Ca^{2+}-free media. Ionomycin (10 μM for 15 s) was used as positive control, n = 3. (G) Representative flow cytometry showing mitochondrial membrane depolarization of MCF-7 control and SPCA2 KD cells. Fenretinide (4-HPR) (10 μM for 20 h) was used as positive control. (H) Mitochondrial membrane depolarization was significantly increased in SPCA2 KD compared to control. n = 3 for control and n = 4 for SPCA2 KD. Significance: $*P < 0.05$, $***P < 0.001$. . (For interpretation of the references to color in this figure legend, the reader is referred to the Web version of this article.)

pathway and leading to cell cycle arrest and apoptosis (Fig. 8E).

3. Discussion

3.1. Multiple mechanisms of Ca^{2+} entry drive cell cycle progression

The coordinated action of Ca^{2+} influx and efflux mechanisms give rise to discrete Ca^{2+} signals that control the re-entry of cells into the cell cycle in early G1 phase, the initiation of DNA synthesis and entry into S-phase [51] and several cell cycle check points at G1/S, G2/M, and metaphase to anaphase transition in mitosis. There is growing evidence that dysregulation of intracellular Ca^{2+} homeostasis underlies multiple hallmarks of cancer, including unchecked proliferation and resistance to apoptosis. Many of the key players in Ca^{2+} regulation of the cell cycle, including ion channels and pumps, and their downstream effectors such as kinases and transcription factors have been identified and their roles in cancer have been extensively reviewed. Despite this intense focus, the role of the secretory pathway Ca^{2+}, Mn^{2+}-ATPase Isoform 2 (SPCA2) had not been considered in cell cycle regulation. Previously, we reported that SPCA2 is prominently elevated in luminal breast cancer subtypes that express ER, PR or HER2 receptors where it interacts with the plasma membrane Orai1 channel to activate constitutive, store-independent Ca^{2+} entry [6,25]. Here, we show that store-independent Ca^{2+} entry (SICE) mediated by SPCA2 is important for cell cycle progression and cell survival by promoting progression through the G1/S checkpoint in breast cancer cells. Similarly, STIM1 and Orai1 or Orai3, mediators of store operated Ca^{2+} entry (SOCE), also promote G1/S transition in cancer cells [52–54]. Thus, both store-independent and store-operated mechanisms of Ca^{2+} entry must be considered as drivers of cancer cell proliferation, offering multiple targets for therapeutic intervention.

3.2. Emerging links between Ca^{2+} homeostasis and p53 signaling

Our transcriptomic analysis revealed that the tumor suppressor p53 pathway mediates cell cycle arrest and apoptosis in the absence of SPCA2, and activates well-known downstream effectors including p21, NOXA and PUMA. Similarly, Orai1 silencing also elicits p21 expression (Figs. S2H–J), and conversely, overexpression of Orai3 was shown to decrease transcriptional activity of p53 in breast cancer cells [55]. Together, these findings reveal a clear link between Ca^{2+} entry and p53 mediated cell cycle arrest and apoptosis. However, the specific molecular pathways connecting Ca^{2+} entry to p53 function appear to be

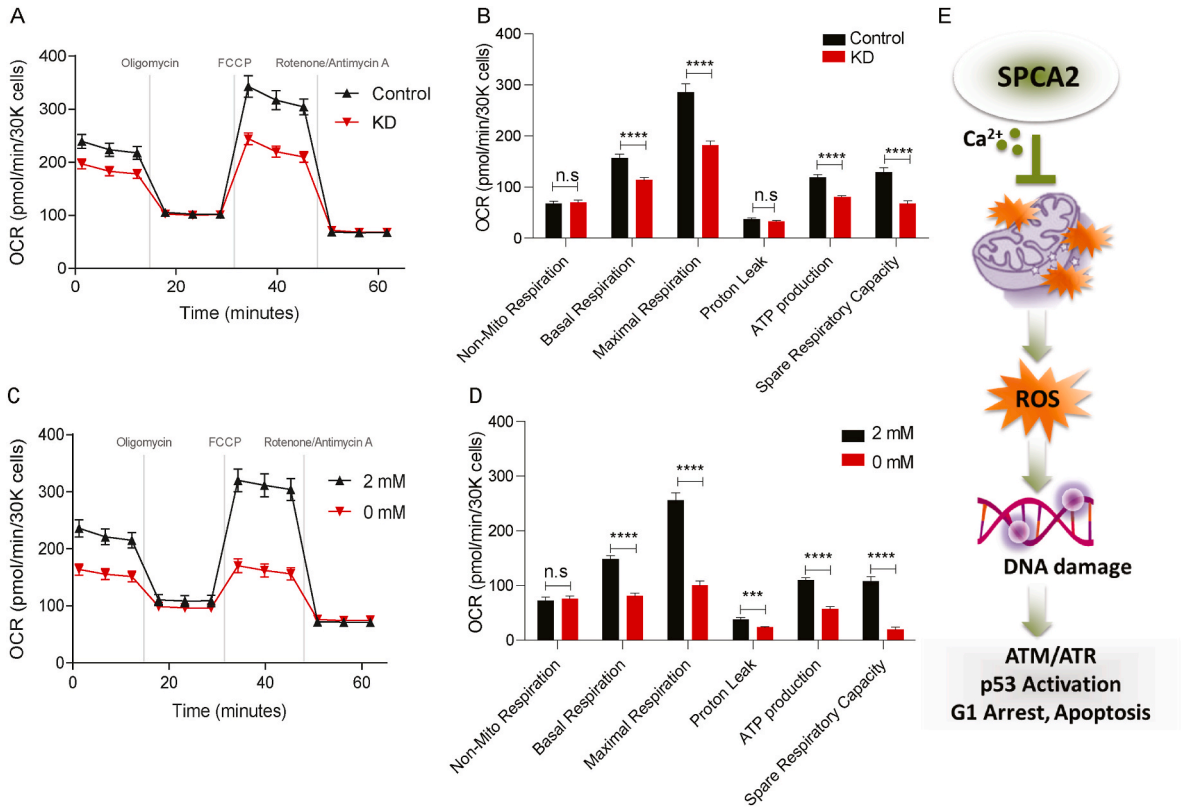

Fig. 8. SPCA2 regulates mitochondrial respiration. (A-B) Oxygen consumption rate (OCR) measurements of MCF-7 control, SPCA2 KD cells, Seahorse XF96e Flux Analyzer with the Mito Stress Test kit under indicated conditions. Basal and maximal OCR were obtained under glucose stimulation after FCCP treatment to uncouple mitochondria. ATP production is defined as basal OCR subtracted by post-oligomycin oxygen consumption. Proton-leak is defined as the difference between oxygen after oligomycin treatment versus after rotenone/antimycin A. Spare respiratory capacity is defined as the difference between maximal respiration and basal respiration. Non-mitochondrial oxygen consumption is the rate after rotenone/antimycin A. Comparisons between MCF-7 control and SPCA2 KD cells (C–D) Oxygen consumption rate (OCR) measurements of MCF-7 cells treated with 2 mM Ca^{2+} and Ca^{2+-}free media (0 mM). Data are presented as mean ± SEM, n = 23. (E) Schematic showing that SPCA2 promotes Ca^{2+} entry into mitochondria. Loss of SPCA2 results in mitochondrial ROS generation and DNA damage, which results in downstream activation of ATM/ATR-p53 pathway, cell cycle arrest and apoptosis. Significance: $^{ns}P > 0.05$, $^{*}P < 0.05$, $^{**}P < 0.01$, $^{***}P < 0.001$, $^{****}P < 0.001$.

diverse, and are not completely understood. In one study, a Ca^{2+}-dependent but transcription-independent role for p53 in regulating apoptosis at the endoplasmic reticulum was reported [56]. Hasna et al. have proposed that Ca^{2+} entry through Orai3 in breast cancer cells signals through the PI3K/Sgk-1/Sek-1 kinases to activate the ubiquitin ligase Nedd4-2, targeting p53 for degradation [55]. Our data show that p53 induced cell cycle arrest and apoptosis in the absence of SPCA2 and SICE occurs downstream of ROS-mediated DNA damage response.

3.3. *Implications of the SPCA2 - p53 axis on DNA damage response in breast cancer*

More than two-third of all breast cancers are ER+, and SPCA2 is up regulated in the majority of these tumors [10]. Although p53 is mutated in >50% of all cancers where it contributes to transformation, most (70–80%) breast cancers lack p53 mutations ($p53^{WT}$) [57]. The mutation status of p53 is especially relevant for the clinical treatment of ER+ breast cancer, which often involves chemotherapy followed by adjuvant therapy consisting of tamoxifen or aromatase inhibitors. In MCF-7 cells, doxorubicin treatment activates p53 to mediate cell death, and there is less p53 activation in doxorubicin resistant cells [58]. This study and others show that Ca^{2+} entry negatively regulates the p53 pathway, either by targeting p53 for degradation or inhibiting upstream activating mechanisms. Thus, therapeutic targeting of SPCA2 or SICE is expected to trigger robust p53 activation in ER+ $p53^{WT}$ breast cancer cells resulting in enhanced sensitivity to DNA damaging agents. Our findings confirm and mechanistically extend a previous report showing that increasing levels of external Ca^{2+} confer doxorubicin resistance in MCF-7 cells [59]. Furthermore, we show that mitochondrial ROS generated by doxorubicin is exacerbated in SPCA2 KD cells and accompanied by decreased levels of MnSOD. Inhibition of MnSOD function may be clinically relevant as high expression of MnSOD was shown to promote survival of circulating breast cancer cells and increase resistance to doxorubicin [60].

Pharmacological targeting of the DNA damage response pathway is of growing interest in cancer therapy [61,62]. In this context, it is significant that store-independent Ca^{2+} entry is required for genomic stability and contributes to resistance against DNA damaging drugs. Genetic predisposition to ovarian and breast tumors is a hallmark of mutations in the BRCA1 and BRCA2 genes that play a critical role in ATM-mediated double stranded DNA break repair. Taken together with clinical data showing poor survival prognosis for ER+/PR+ breast cancer patients expressing high SPCA2, our findings should motivate a search for drugs that target components of store-independent Ca^{2+} entry pathway in hormone receptor positive breast cancer cells and potentially synergize with DDR pathway inhibitors.

3.4. *Store independent mechanism of mitochondrial Ca^{2+} entry*

This study revealed an unexpected role for SPCA2 in mitochondrial Ca^{2+} homeostasis and function: mitochondrial Ca^{2+} levels were significantly depleted in the absence of SPCA2. We observed loss of mitochondrial membrane potential and mitochondrial respiration in the absence of SPCA2 and extracellular Ca^{2+}. Furthermore, SICE was

required for optimal expression of the mitochondrial-specific manganese superoxide dismutase (MnSOD/SOD2), which could account for increased mitochondrial ROS accumulation in the absence of SPCA2. The specific temporal sequence of events linking loss of store-independent Ca^{2+} entry to mitochondrial dysfunction remains to be determined. We note the interdependence of many mitochondrial phenotypes: for example, Ca^{2+} is required for activation of dehydrogenases in the respiratory chain and generation of the inside-negative potential across the inner mitochondrial membrane (IMM). In turn, the membrane potential is a significant driving force for Ca^{2+} uptake through the MCU complex in the IMM. It is likely that specific and dynamic tethering sites between the plasma membrane, secretory vesicles and mitochondria promote microdomains of high Ca^{2+} concentration, mediating efficient transfer of Ca^{2+} into the mitochondria. These tethering sites have been most extensively described at ER-PM and ER-mitochondrial junctions [3]. Similarly, identification of the ultra-structural organization and molecular composition of juxtaposed membranes that potentially mediate store-independent Ca^{2+} entry mechanisms could help decipher the complex and dynamic cross talk between organelles.

4. Methods and materials

4.1. Cell culture

Cells used in this study were MCF-7 (ATCC HTB-22), MCF-10A (ATCC CRL-10317), MDA-MB-231 (ATCC HTB-26), Hs578T (ATCC HTB-126), and ZR-75 (gifted by Dr. Nakshatri, Indiana University School of Medicine). MCF-7, MDA-MB-231 and Hs578T cells were gown in DMEM (Thermo Fisher Scientific, Waltham, MA) containing antibiotic, and 5% FBS (Sigma Aldrich, St. Louis, MO). For calcium free experiments, cells were grown in calcium free DMEM, with 2.5% FBS and 150 μM EGTA [55]. MCF-10A was cultured in DMEM/F12 containing 5% horse serum, 20 ng/mL EGF, 0.5 mg/mL hydrocortisone, 100 ng/mL cholera toxin, 10 μg/mL insulin, and 1X penicillin/streptomycin. ZR-75 was cultured RPMI 1640 containing antibiotic, and 10% FBS. Cells were cultured with 5% CO_2 and at 37 °C in a humidified incubator. All cell lines were grown for less than a month or no more than 6 passages to avoid cross contamination. We did not see visible contamination by mycoplasma. Since SPCA2 expression is regulated by cell density [25], cells were maintained at 50–60% confluency in both knockdown experiments and controls. Although we used lentiviral transfection, resistant clones tended to appear after 2–3 passages, therefore all experiments used early passage cells.

4.2. Lentiviral transfection

The silencing resistant SPCA2R construct has been previously described [10,25]. The non-targeting shRNA sequence used as negative control was CAACAAGATGAAGAGCACCAA (Sigma-Aldrich). FUGW overexpression constructs and pLK0.1 shRNA and lentiviral construction of both SPCA isoforms were packaged and transfected according to previous methods [25] using pCMV-Δ8.9 and PMDG at a ratio using 9:8:1 in HEK293T cells. Virus was collected after 24 h for 3 consecutive days and concentrated with Lenti-X Concentrator (Takara Bio USA, Mountain View, CA). A mixture of two shRNA constructs for SPCA2 was used. Cells were transfected with virus for 48 h, and selected with puromycin at varying concentrations according to kill curves performed for each specific cell line (0.5–2 μg/mL). Knockdowns were confirmed by qPCR. Experiments were performed within 2–3 passages to ensure that knockdown was maintained.

4.3. TP53 knockout in MCF-7 cells

TP53 knockout MCF-7 cells were generated as previously published [63]. Human codon-optimized *Streptococcus pyogenes* wild type Cas9 (Cas9-2A-GFP) was obtained from Addgene (Cambridge, MA). Chimeric guide RNA expression cassettes with different sgRNAs (sgRNA1: CCATTGTTCAATATCGTCCG; sgRNA3: TGGTTATAGGATTCAACCGG) were ordered as gBlocks. These gBlocks were amplified by PCR using primers: gBlock_Amplifying_F: 5′-GTACAAAAAAGCAGGCTTTAAAGG-3′ and gBlock_Amplifying_R: 5′-TAATGCCAACTTTGTACAAGAAAGC-3′. The PCR product was purified by Agencourt Ampure XP PCR Purification beads per the manufacturer's protocol (Beckman Coulter, Brea, CA). One microgram of Cas9 plasmid and 0.3 μg of each gRNA gBlock (pair: sgRNA1 & sgRNA3) were cotransfected into MCF-7 cells via Lipofectamine 3000 in a 6-well plate. Knockout cells created using the pair sgRNA1 & sgnRNA3 were named KO3.4. The knockout pool was cultured in 10 μM Nutlin-3a (SelleckChem, Houston, TX) for 2 months, changing nutlin-3a treated media every 3 days and passaging cells every 6–8 days. The isogenic clone KO3.4E1 was isolated from the knockout pool via limiting dilution in a 96-well plate and incubated at 37 °C in a CO_2 incubator for 15 days.

DNA was isolated from each MCF-7 wild type and knockout single cell clones following the Agencourt DNAdvance genomic DNA isolation kit. MCF-7 KO3.4E1 cells were PCR amplified using primers: TP53_exon_4_F and TP53_Woke_R: 5′-ATTAGGCCCCTCCTTGAGAC-3'. Products were sent to Eton Bioscience Inc. who purified the PCR products and performed Sanger Sequencing.

4.4. Cell proliferation

MTS growth assays were performed on adherent cells by plating 1000–5000 cells per well in a 96-well plate and assaying using CellTiter 96® AQueous One Solution (Promega, Madison, WI) and incubating for 2 h and reading at 490 nm. To confirm the effect of SPCA2 KD and rescue on cell proliferation, BrdU incorporation was determined using BrdU Cell Proliferation Kit (Abcam, Cambridge, UK). About 0.15 million MCF-7 cells were seeded into 96-well plates. After 2 h BrdU was added into the wells for 24 h. Further steps are carried according to the manufacturer's protocol.

For MCF-10A and ZR-75 knockdown experiments and MCF-7 SPCA2 ectopic expression experiments, 0.3 million cells were platted in a 6 well dish and cell proliferation was measured using trypan blue (Invitrogen, Carlsbad, CA) staining. Trypan blue staining was also used to measure viability of cells treated with SKF-96365. Based on doubling time of each cell line, proliferation was measured at different days.

4.5. Cell cycle analysis

Cell cycle analysis was performed by dissociating adherent cells and fixing them in 4% paraformaldehyde for 30 min on ice. For better nuclear staining, fixed cells were then frozen for 1–2 weeks and thawed on ice and washed with PBS. Cells were treated with 100 μg/ml of RNAse A (Thermo Fisher Scientific) and stained with 50 μg/ml propidium iodide (Invitrogen) prior to running flow cytometry via FACSAria (BD Biosciences, San Jose, CA). The shoulder of sub-haploid nuclear staining cells was excluded during flow cytometry gating to focus on cell cycle distribution.

4.6. cDNA synthesis & quantitative PCR

1 μg of RNA was collected and used for cDNA synthesis (Applied Biosystems, Foster City, CA). The qPCR mastermix was obtained from Thermo Fischer Scientific, 50 ng of cDNA, and Taqman probe (Thermo Fischer Scientific) as specified; GAPDH (Hs02796624_g1), SPCA2 (Hs00939492_m1), SPCA1 (Hs00995930_m1), PUMA (Hs00248075_m1), p21 (Hs00355782_m1), and NOXA (Hs00560402_m1).

4.7. Apoptosis assays

TUNEL assay: Apoptosis was measured using terminal deoxynucleotidyl transferase dUTP nick end labeling (TUNEL) assay (APO-

DIRECT Kit, BD Biosciences) in conjunction with propidium iodide staining. After treatment, cells were fixed in 1% (w/v) paraformaldehyde (Affymetrix, Santa Clara, CA) in PBS and stored in 70% ethanol at −20 °C for 24 h. Cells were rinsed with 1X PBS and incubated with 50 μL of the DNA labeling solution for 3 h at 37 °C. After incubation, cells were washed twice and suspended in 500 μL of propidium iodide/RNase staining buffer for 30 min of counterstaining, then analyzed with flow cytometry (BD LSR-II, BD Biosciences). Data analysis was performed using FlowJo software (Ashland, OR) and plotted using GraphPad Prism (La Jolla, CA).

Annexin V: According to the manufacturer's protocol, cells were trypsinized and washed with PBS. Cells were then washed in annexin binding buffer (ThermoFisher) and stained with annexin V for 15 min. Stained cells were then diluted 1:5 in binding buffer and analyzed by flow cytometry using FACSAria.

Immunofluorescence of cleaved caspase-3: Cells were cultured on glass coverslips and were rinsed with PBS and pre-extracted with 1X PHEM buffer, 8% sucrose and 0.025% saponin. Cells were fixed with 4% paraformaldehyde for 30 min and were rinsed and washed with PBS 3 times for 5 min each. After blocking in 1% BSA, cells were incubated with overnight in 4 °C using cleaved caspase-3 (Asp175) Antibody (Cell Signaling Technologies, Danvers, MA). Cells were rinsed with 0.2% BSA 3 times for 5 min and were then incubated with a fluorescent secondary antibody in 1% BSA and 0.025% saponin buffer for 30 min at room temperature. Coverslips were washed and mounted onto slides with mounting media (Agilent, Santa Clara, CA). Immunofluorescent staining was analyzed using ImageJ.

4.8. Western blotting

Cells were collected, and lysed in RIPA buffer (Thermo Fisher Scientific) supplemented with protease inhibitor cocktail, and phosphatase inhibitors. Protein quantification was done by the bicinchoninic acid assay. Thirty μg of protein in each sample was resolved by electrophoresis using 4–12% bis-tris gels (Thermo Fisher Scientific) and transferred to nitrocellulose membrane (Bio-Rad, Hercules, CA). Immunoblots were probed with antibodies (1:1000) from Cell Signaling Technologies, followed by incubation with HRP-conjugated secondary antibodies. Proteins were visualized using chemiluminescence substrate. Blots were analyzed using ImageJ.

4.9. Live cell calcium imaging

Live imaging of Ca^{2+} was performed using Fura2- AM (Invitrogen) [25]. MDA-MB-231 cells with or without SPCA2R and SPCA2D379N (Control n = 51 cells, SPCA2R n = 50 cells, SPCA2D379N = 39) were treated with Fura2-AM in imaging buffer (20 mM Hepes, 126 mM, NaCl, 4.5 mM KCl, 2 mM $MgCl_2$, 10 mM glucose at pH 7.4) for 30 min. Cells were excited at 340 nm and 380 nm, and Fura emission was captured at 505 nm. To show store independent Ca^{2+} entry (SICE), cells were briefly washed in nominally Ca^{2+}-free buffer followed by addition of Ca^{2+} (2 mM). Baseline readings in calcium-free conditions were established for 80 s and then cells were recorded under 2 mM Ca^{2+} conditions for 6 min.

4.10. Microarray analysis

RNA was isolated using QIAGEN's RNEasy Mini (Qiagen, Germantown, MD) manufacturer's protocol. Samples were submitted to the Johns Hopkins Transcriptomics and Deep Sequencing Core for expression analysis. The mRNA concentrations and integrity were determined with Agilent's NanoDrop instrument then amplified and biotinylated with the Affymetrix GeneChip 3′ IVT PLUS Reagent kit (ThermoFisher Scientific) following manufacturer's protocol. The labeled samples were then hybridized to Affymetrix Human Genome U133 Plus 2.0 Array GeneChips (ThermoFisher Scientific, Waltham MA) and scanned Using Affymetrix' GeneChip Scanner 3000 7G and default parameters. Raw data generated as CEL files by the Affymetrix Expression Console were imported for normalization and analysis into Partek Genomics Suite v7.0 (Partek Inc. St Louis MO, USA). Data were extracted using the Affymetrix na36 transcript annotation, log_2 transformed, and quantile normalized with the RMA (Robust Multi-Array Average) algorithm. This yielded data for 44.6K transcripts, 21K unique NCBI Entrez genes, whose annotation was subsequently updated to current HGNC/NCBI nomenclature. After data quality control the samples' gene expression were independently compared using a two tailed one way ANOVA between their shSPCA2_1Way vs. control MCF7 biological classes, which provided relative levels of gene expression and statistical significance, as fold change and imputed p-value respectively. Genes whose log_2 fold changes were greater than 2SD from the mean were deemed to be differentially expressed.

4.11. Detection of DNA damage

Single stranded DNA damage: Cells were fixed in methanol-PBS (6:1) and analyzed 1–3 days after fixation. Staining with F7-26 monoclonal antibody (Millipore Sigma, Burlington, MA) was performed according to manufacturer's instructions [64]: Fixed cells were resuspended in 0.25 ml of formamide and heated in a water bath at 75 °C for 10 min. The cells were then returned to room temperature and washed with 2 ml of 1% nonfat dry milk in PBS for 15 min, resuspended in 100 μl of anti-ssDNA Mab F7-26 (100 μg (0.5 ml) antibody in 4.5 ml of 5% FBS in PBS) or 100 μl of isotype control (IgM) Mab (10 μg/ml), incubated at room temperature for 25 min, washed with PBS, and then stained with 100 μl of fluorescence-conjugated goat anti-mouse IgM antibody (1:50 in 1% nonfat dry milk in PBS) for 25 min at room temperature. Cells were filtered 0.7 μm cell filter to filter the cell debris. Cells were then washed with PBS and resuspended in 0.5 ml of PBS containing 1 μg/ml propidium iodide (PI) and 50 μg RNase and analyzed by flow cytometry (BD LSR-II) MCF-7 cells were exposed to 10 Gy γ radiation, were used as a positive control.

Double stranded DNA damage: Double standard DNA breaks were detected using p-H2AX (Ser139) antibody (Cell Signaling Technologies) using Immunofluorescence and western blotting method mentioned above.

4.12. Cytotoxicity assay

MTT assay was used to measure cytotoxicity. Cells were seeded at ~3000–10,000 cells/well in 96 well plates. After the cells were incubated overnight, they were treated with drugs. Drugs (obtained from Selleck chemicals or Sigma-Aldrich) were dosed from clinically achievable low to high concentrations, and four to six replicate wells were tested per concentration. Cells were treated with drugs for 48–120 h (120 h for SPCA2 KD in MCF-7 and MCF-10A cells, 48 h for calcium-free experiments, and 72 h for MCF-7 SPCA2R experiment). Thereafter, MTT dye (Thermo Fisher Scientific) was added to the cells for 4 h, and SDS-HCl solution was added to each well and mixed thoroughly. After 4 h of incubation, absorbance was measured at 570 nm. Cell survival is calculated as the percentage normalized to control.

4.13. ROS measurement

ROS was measured using DCFDA dye (Thermo Fisher Scientific) using flow cytometry (BD LSR-II). Control and knockdown cells were washed with PBS and incubated with DCFDA dye (10 μM) for 30 min at 37 °C. After incubation, cells were washed twice and suspended in 500 μL of PBS, then analyzed with flow cytometry. Data analysis was performed using FlowJo software. H_20_2 was used as a positive control. Mitochondrial ROS was measured using MitoSOX-Red (Thermo Fisher Scientific) using flow cytometry (BD LSR-II). Control and knockdown cells were washed with PBS and incubated with MitoSOX-Red dye (10 μM) for 30 min at 37 °C. After incubation, cells were washed twice and

suspended in 500 μL of PBS, then analyzed with flow cytometry. Data analysis was performed using FlowJo software. Doxorubicin was used as a positive control.

4.14. Mitochondrial Ca^{2+} measurement

Mitochondrial calcium was measured using Rhod-2 AM dye (Abcam) using flow cytometry (BD LSR-II) and microscopy. For flow cytometry, control and knockdown cells were washed with PBS and incubated with Rhod-2 AM dye (5 μM) for 30 min at 37 °C. After incubation, cells were washed twice and suspended in 500 μL of PBS, then analyzed with flow cytometry. Data analysis was performed using FlowJo software. Ionomycin was used as a positive control. For microscopy, cells were grown in coverslips, washed and incubated with 5 μM of Rhod-2 AM dye and 1 μM of MitoTracker green (Cell Signaling Technologies) for 30 min in live cell calcium imaging solution (Invitrogen). Cells were then washed with PBS, and incubated in 1% paraformaldehyde and mounted for confocal microscopy.

4.15. Analysis of mitochondrial membrane potential

Cells (control and SPCA2 KD) were resuspended in 1 mL medium containing 5 μM JC-1 mitochondrial membrane potential probe (Thermo Fisher Scientific). After incubation at 37 °C for 30 min, cells were washed twice and suspended in 500 μL of PBS cells, and analyzed by flow cytometry. Percentage of cells exhibiting red and green fluorescence was quantified. The chemopreventive drug *N*-(4-hydroxyphenyl)retinamide (4-HPR, fenretinide) is known to cause ROS-induced mitochondrial depolarization [49,50] and was used as a positive control. Cells were treated with 10 μM 4-HPR for 20 h prior to flow cytometry analysis.

4.16. Oxygen consumption measurements

Cells were seeded onto XF96 cell culture microplate coated with 0.001% (w/v) poly-D-lysine (Sigma-Aldrich) at 30,000 cells/well and incubated overnight. For calcium free treatment, cells were exposed to calcium free DMEM, with 2.5% FBS and 150 μM EGTA for 10 min, washed and incubated with calcium free DMEM, 2.5% FBS without EGTA overnight. Cells were washed twice with Seahorse XF DMEM Basal Medium supplemented with 10 mM glucose, 2 mM L-glutamine, and 1 mM sodium pyruvate and preincubated for 1 h in a 37 °C humidified CO_2-free incubator.

Oxygen consumption rate (OCR) was measured by a Seahorse XF96e FluxAnalyzer with the Mito Stress Test kit (Agilent Technologies, Santa Clara, CA). The Mito Stress Test inhibitors were injected during the measurements as follows; oligomycin (2 μM), FCCP (0.5 μM), rotenone and antimycin A (0.5 μM). The OCR values were normalized to cell density determined by the CyQUANT Cell Proliferation Assay Kit (Invitrogen) according to the manufacture's instruction.

4.17. Flow analysis

Flow data analysis was performed using FlowJo software. Forward versus side scatter (FSC-A vs SSC-A) gating is used to identify cells of interest based on size and granularity. Since doublet cells can significantly affect analysis and could lead to inaccurate conclusions. A forward scatter height (FSC–H) vs. forward scatter area (FSC-A) or forward scatter width (FSC–W) vs. forward scatter (FSC-A) area density plot was used to exclude doublets. Doublets were future gated out by using side scatter density plots similar to forward scatter. Single parameter histograms were used to further identify distinct cell types that express a particular marker in a specific population of cells.

4.18. Statistical analysis

Student t-test was used to determine significance between two groups. To perform statistical analysis experiments were performed in biological triplicates (n = 3). Tests were considered significant at $P < 0.05$. Significance and non-significance was shown as ^{ns} $P > 0.05$, $^{*}P < 0.05$, $^{**}P < 0.01$, $^{***}P < 0.001$, $^{****}P < 0.0001$.

Availability of data and material

Microarray data have been deposited in NCBI's Gene Expression Omnibus and are accessible through GEO Series accession number GSE148537 (https://www.ncbi.nlm.nih.gov/geo/query/acc.cgi?acc=GSE148537).

Funding

M.R.M. is an AACR Astrazeneca Fellow. M.J.K. is a recipient of Ruth L. Kirschstein Individual National Research Service Award F31CA220967. A.X.M. is a recipient of the Howard Hughes Medical Institute predoctoral Gilliam Fellowship. N.S. is supported by an Award from the American Heart Association and the Barth Syndrome Foundation (Award ID: 828058). S.M.C. is supported by grants from the NIH (R01GM111548). R.R. is supported by grants from the NIH (R01DK108304) and BSF (13044).

Author contributions

M.R.M performed most experiments, including p53 signaling, ROS generation, DNA damage responses, drug toxicity, mitochondrial calcium and depolarization. M.J.K performed microscopy and image analysis for caspase. D.K.D performed cell cycle analysis and Ca^{2+} flux. J.W. and P.B. constructed and validated the TP53 mutant. A.X.M. and C. C.T analyzed the microarray data. N.S measured oxygen consumption rates, and SMC advised on experimental design of mitochondrial respiration experiments. M.R.M and R.R. wrote the paper, and all authors contributed to making the figures and editing the text.

Declaration of competing interest

None.

Acknowledgements

M.R.M. acknowledges the support of American Association of Indian Scientists in Cancer Research. M.J.K and A.X.M. acknowledge the support of the graduate training programs in Cellular & Molecular Medicine and Biochemistry Cell and Molecular Biology, respectively, at the Johns Hopkins University. We would like to thank the Johns Hopkins Transcriptomics and Deep Sequencing Core for completing the microarray analysis. Authors like to thank James Osei Owusu for technical advice.

Appendix A. Supplementary data

Supplementary data to this article can be found online at https://doi.org/10.1016/j.redox.2022.102240.

References

[1] M.J. Berridge, M.D. Bootman, H.L. Roderick, Calcium signalling: dynamics, homeostasis and remodelling, Nat. Rev. Mol. Cell Biol. 4 (7) (2003) 517–529.
[2] D.E. Clapham, Calcium signaling, Cell 131 (6) (2007) 1047–1058.
[3] I. Annunziata, A. d'Azzo, Interorganellar membrane microdomains: dynamic platforms in the control of calcium signaling and apoptosis, Cells 2 (3) (2013) 574–590.
[4] H.L. Roderick, S.J. Cook, Ca2+ signalling checkpoints in cancer: remodelling Ca2+ for cancer cell proliferation and survival, Nat. Rev. Cancer 8 (5) (2008) 361–375.

[5] A. Gorlach, K. Bertram, S. Hudecova, O. Krizanova, Calcium and ROS: a mutual interplay, Redox Biol. 6 (2015) 260–271.
[6] M.R. Makena, R. Rao, Subtype specific targeting of calcium signaling in breast cancer, Cell Calcium (2019) 102109.
[7] A. Bergner, R.M. Huber, Regulation of the endoplasmic reticulum Ca(2+)-store in cancer, Anti Cancer Agents Med. Chem. 8 (7) (2008) 705–709.
[8] G.R. Monteith, D. McAndrew, H.M. Faddy, S.J. Roberts-Thomson, Calcium and cancer: targeting Ca2+ transport, Nat. Rev. Cancer 7 (7) (2007) 519–530.
[9] N. Prevarskaya, R. Skryma, Y. Shuba, Targeting Ca(2)(+) transport in cancer: close reality or long perspective? Expert Opin. Ther. Targets 17 (3) (2013) 225–241.
[10] D. Dang, H. Prasad, R. Rao, Secretory pathway Ca2+-ATPases promote in vitro microcalcifications in breast cancer cells, Mol. Carcinog. 56 (11) (2017) 2474–2485.
[11] V. Castronovo, A. Bellahcene, Evidence that breast cancer associated microcalcifications are mineralized malignant cells, Int. J. Oncol. 12 (2) (1998) 305–308.
[12] J.A. Godoy, J.A. Rios, P. Picon-Pages, V. Herrera-Fernandez, B. Swaby, G. Crepin, R. Vicente, J.M. Fernandez-Fernandez, F.J. Munoz, Mitostasis, calcium and free radicals in health, aging and neurodegeneration, Biomolecules 11 (7) (2021).
[13] C. Giorgi, S. Marchi, P. Pinton, The machineries, regulation and cellular functions of mitochondrial calcium, Nat. Rev. Mol. Cell Biol. 19 (11) (2018) 713–730.
[14] D.M. Shin, S. Muallem, What the mitochondria see, Mol. Cell. 39 (1) (2010) 6–7.
[15] M. Giacomello, I. Drago, M. Bortolozzi, M. Scorzeto, A. Gianelle, P. Pizzo, T. Pozzan, Ca2+ hot spots on the mitochondrial surface are generated by Ca2+ mobilization from stores, but not by activation of store-operated Ca2+ channels, Mol. Cell. 38 (2) (2010) 280–290.
[16] B.M. Cross, A. Hack, T.A. Reinhardt, R. Rao, SPCA2 regulates Orai1 trafficking and store independent Ca2+ entry in a model of lactation, PLoS One 8 (6) (2013), e67348.
[17] H.M. Faddy, C.E. Smart, R. Xu, G.Y. Lee, P.A. Kenny, M. Feng, R. Rao, M.A. Brown, M.J. Bissell, S.J. Roberts-Thomson, G.R. Monteith, Localization of plasma membrane and secretory calcium pumps in the mammary gland, Biochem. Biophys. Res. Commun. 369 (3) (2008) 977–981.
[18] J. Vanoevelen, L. Dode, K. Van Baelen, R.J. Fairclough, L. Missiaen, L. Raeymaekers, F. Wuytack, The secretory pathway Ca2+/Mn2+-ATPase 2 is a Golgi-localized pump with high affinity for Ca2+ ions, J. Biol. Chem. 280 (24) (2005) 22800–22808.
[19] M. Xiang, D. Mohamalawari, R. Rao, A novel isoform of the secretory pathway Ca2+,Mn(2+)-ATPase, hSPCA2, has unusual properties and is expressed in the brain, J. Biol. Chem. 280 (12) (2005) 11608–11614.
[20] M. Feng, D.M. Grice, H.M. Faddy, N. Nguyen, S. Leitch, Y. Wang, S. Muend, P. A. Kenny, S. Sukumar, S.J. Roberts-Thomson, G.R. Monteith, R. Rao, Store-independent activation of Orai1 by SPCA2 in mammary tumors, Cell 143 (1) (2010) 84–98.
[21] M.A. Fenech, M.M. Carter, P.B. Stathopulos, C.L. Pin, The pancreas-specific form of secretory pathway calcium ATPase 2 regulates multiple pathways involved in calcium homeostasis, Biochim. Biophys. Acta Mol. Cell Res. 1867 (1) (2020) 118567.
[22] S. Smaardijk, J. Chen, S. Kerselaers, T. Voets, J. Eggermont, P. Vangheluwe, Store-independent coupling between the secretory pathway Ca(2+) transport ATPase SPCA1 and Orai1 in Golgi stress and Hailey-Hailey disease, Biochim. Biophys. Acta Mol. Cell Res. 1865 (6) (2018) 855–862.
[23] C. Cantonero, J. Sanchez-Collado, M.A. Gonzalez-Nunez, G.M. Salido, J.J. Lopez, I. Jardin, J.A. Rosado, Store-independent Orai1-mediated Ca(2+) entry and cancer, Cell Calcium 80 (2019) 1–7.
[24] B.M. Cross, G.E. Breitwieser, T.A. Reinhardt, R. Rao, Cellular calcium dynamics in lactation and breast cancer: from physiology to pathology, Am. J. Physiol. Cell Physiol. 306 (6) (2014) C515–C526.
[25] D.K. Dang, M.R. Makena, J.P. Llongueras, H. Prasad, M. Ko, M. Bandral, R. Rao, A Ca2+-ATPase Regulates E-Cadherin Biogenesis and Epithelial–Mesenchymal Transition in Breast Cancer Cells, Molecular Cancer Research, 2019.
[26] K. Fernald, M. Kurokawa, Evading apoptosis in cancer, Trends Cell Biol. 23 (12) (2013) 620–633.
[27] G.E. Shull, M.L. Miller, V. Prasad, Secretory pathway stress responses as possible mechanisms of disease involving Golgi Ca2+ pump dysfunction, Biofactors 37 (3) (2011) 150–158.
[28] L. Dode, J.P. Andersen, J. Vanoevelen, L. Raeymaekers, L. Missiaen, B. Vilsen, F. Wuytack, Dissection of the functional differences between human secretory pathway Ca2+/Mn2+-ATPase (SPCA) 1 and 2 isoenzymes by steady-state and transient kinetic analyses, J. Biol. Chem. 281 (6) (2006) 3182–3189.
[29] M.R. Makena, M. Ko, D.K. Dang, R. Rao, Epigenetic modulation of SPCA2 reverses epithelial to mesenchymal transition in breast cancer cells, Cancers 13 (2) (2021) 259.
[30] M. Feng, D.M. Grice, H.M. Faddy, N. Nguyen, S. Leitch, Y. Wang, S. Muend, P. A. Kenny, S. Sukumar, S.J. Roberts-Thomson, Store-independent activation of Orai1 by SPCA2 in mammary tumors, Cell 143 (1) (2010) 84–98.
[31] Y.F. Chen, P.C. Lin, Y.M. Yeh, L.H. Chen, M.R. Shen, Store-operated Ca(2+) entry in tumor progression: from molecular mechanisms to clinical implications, Cancers 11 (7) (2019).
[32] X. Mai, J. Shang, S. Liang, B. Yu, J. Yuan, Y. Lin, R. Luo, F. Zhang, Y. Liu, X. Lv, C. Li, X. Liang, W. Wang, J. Zhou, Blockade of Orai1 store-operated calcium entry protects against renal fibrosis, J. Am. Soc. Nephrol. 27 (10) (2016) 3063–3078.
[33] J. Chen, The cell-cycle arrest and apoptotic functions of p53 in tumor initiation and progression, Cold Spring Harbor Perspect. Med. 6 (3) (2016) a026104.
[34] M.H. Kang, C.P. Reynolds, Bcl-2 inhibitors: targeting mitochondrial apoptotic pathways in cancer therapy, Clin. Cancer Res. 15 (4) (2009) 1126–1132.
[35] Y. Shiloh, ATM and ATR: networking cellular responses to DNA damage, Curr. Opin. Genet. Dev. 11 (1) (2001) 71–77.
[36] H.J. Burstein, D. Hayes, S. Vora, Adjuvant Chemotherapy for HER2-Negative Breast Cancer, 2017.
[37] A.F. Schott, Systemic Treatment of Metastatic Breast Cancer in Women: Chemotherapy, Wolters Kluwer UpToDate, 2015.
[38] S. Yan, M. Sorrell, Z. Berman, Functional interplay between ATM/ATR-mediated DNA damage response and DNA repair pathways in oxidative stress, Cell. Mol. Life Sci. 71 (20) (2014) 3951–3967.
[39] N. Kaludercic, S. Deshwal, F. Di Lisa, Reactive oxygen species and redox compartmentalization, Front. Physiol. 5 (2014) 285.
[40] S.R. Alam, H. Wallrabe, Z. Svindrych, A.K. Chaudhary, K.G. Christopher, D. Chandra, A. Periasamy, Investigation of mitochondrial metabolic response to doxorubicin in prostate cancer cells: an NADH, FAD and tryptophan FLIM assay, Sci. Rep. 7 (1) (2017) 1–10.
[41] Y. Jiao, S. Ma, Y. Wang, J. Li, L. Shan, Q. Liu, Y. Liu, Q. Song, F. Yu, H. Yu, H. Liu, L. Huang, J. Chen, N-acetyl cysteine depletes reactive oxygen species and prevents dental monomer-induced intrinsic mitochondrial apoptosis in vitro in human dental pulp cells, PLoS One 11 (1) (2016), e0147858.
[42] V.H. Guaiquil, J.C. Vera, D.W. Golde, Mechanism of vitamin C inhibition of cell death induced by oxidative stress in glutathione-depleted HL-60 cells, J. Biol. Chem. 276 (44) (2001) 40955–40961.
[43] M.R. Makena, B. Koneru, T.H. Nguyen, M.H. Kang, C.P. Reynolds, Reactive oxygen species–mediated synergism of fenretinide and romidepsin in preclinical models of T-cell lymphoid malignancies, Mol. Cancer Therapeut. 16 (4) (2017) 649–661.
[44] M.R. Makena, T.H. Nguyen, B. Koneru, A. Hindle, W.-H. Chen, D.U. Verlekar, M. H. Kang, C.P. Reynolds, Vorinostat and Fenretinide Synergize in Preclinical Models of T-Cell Lymphoid Malignancies, Anti-Cancer Drugs, 2020.
[45] M.P. Murphy, How mitochondria produce reactive oxygen species, Biochem. J. 417 (1) (2009) 1–13.
[46] C. Dejos, D. Gkika, A.R. Cantelmo, The two-way relationship between calcium and metabolism in cancer, Front. Cell Dev. Biol. 8 (2020) 1251.
[47] J.T. Maxwell, C.H. Tsai, T.A. Mohiuddin, J.Q. Kwong, Analyses of mitochondrial calcium influx in isolated mitochondria and cultured cells, JoVE 134 (2018).
[48] F. Sivandzade, A. Bhalerao, L. Cucullo, Analysis of the mitochondrial membrane potential using the cationic JC-1 dye as a sensitive fluorescent probe, Bio Protoc. 9 (1) (2019).
[49] M.M. Song, M.R. Makena, A. Hindle, B. Koneru, T.H. Nguyen, D.U. Verlekar, H. Cho, B.J. Maurer, M.H. Kang, C.P. Reynolds, Cytotoxicity and molecular activity of fenretinide and metabolites in T-cell lymphoid malignancy, neuroblastoma, and ovarian cancer cell lines in physiological hypoxia, Anti Cancer Drugs 30 (2) (2019) 117–127.
[50] R. Cuperus, R. Leen, G.A. Tytgat, H.N. Caron, A.B. van Kuilenburg, Fenretinide induces mitochondrial ROS and inhibits the mitochondrial respiratory chain in neuroblastoma, Cell. Mol. Life Sci. : CMLS 67 (5) (2010) 807–816.
[51] N. Takuwa, W. Zhou, Y. Takuwa, Calcium, calmodulin and cell cycle progression, Cell. Signal. 7 (2) (1995) 93–104.
[52] M. Faouzi, F. Hague, M. Potier, A. Ahidouch, H. Sevestre, H. Ouadid-Ahidouch, Down-regulation of Orai3 arrests cell-cycle progression and induces apoptosis in breast cancer cells but not in normal breast epithelial cells, J. Cell. Physiol. 226 (2) (2011) 542–551.
[53] Y. Sun, X. Cui, J. Wang, S. Wu, Y. Bai, Y. Wang, B. Wang, J. Fang, Stromal interaction molecule 1 (STIM1) silencing inhibits tumor growth and promotes cell cycle arrest and apoptosis in hypopharyngeal carcinoma, Med. Oncol. 32 (5) (2015) 150.
[54] Y.W. Chen, Y.F. Chen, Y.T. Chen, W.T. Chiu, M.R. Shen, The STIM1-Orai1 pathway of store-operated Ca2+ entry controls the checkpoint in cell cycle G1/S transition, Sci. Rep. 6 (2016) 22142.
[55] J. Hasna, F. Hague, L. Rodat-Despoix, D. Geerts, C. Leroy, D. Tulasne, H. Ouadid-Ahidouch, P. Kischel, Orai3 calcium channel and resistance to chemotherapy in breast cancer cells: the p53 connection, Cell Death Differ. 25 (4) (2018) 693–707.
[56] J. Miciak, F. Bunz, Long story short: p53 mediates innate immunity, Biochim. Biophys. Acta 1865 (2) (2016) 220–227.
[57] P. Bertheau, J. Lehmann-Che, M. Varna, A. Dumay, B. Poirot, R. Porcher, E. Turpin, L.F. Plassa, A. de Roquancourt, E. Bourstyn, P. de Cremoux, A. Janin, S. Giacchetti, M. Espie, H. de The, p53 in breast cancer subtypes and new insights into response to chemotherapy, Breast 22 (Suppl 2) (2013) S27–S29.
[58] E.M. Saleh, R.A. El-Awady, M.A. Abdel Alim, A.H. Abdel Wahab, Altered expression of proliferation-inducing and proliferation-inhibiting genes might contribute to acquired doxorubicin resistance in breast cancer cells, Cell Biochem. Biophys. 55 (2) (2009) 95–105.
[59] T.T.T. Nguyen, Y.J. Lim, M.H.M. Fan, R.A. Jackson, K.K. Lim, W.H. Ang, K.H. K. Ban, E.S. Chen, Calcium modulation of doxorubicin cytotoxicity in yeast and human cells, Gene Cell. 21 (3) (2016) 226–240.
[60] A. Fu, S. Ma, N. Wei, B.X.X. Tan, E.Y. Tan, K.Q. Luo, High expression of MnSOD promotes survival of circulating breast cancer cells and increases their resistance to doxorubicin, Oncotarget 7 (31) (2016) 50239.
[61] L. Carrassa, G. Damia, DNA damage response inhibitors: mechanisms and potential applications in cancer therapy, Cancer Treat Rev. 60 (2017) 139–151.

[62] M.J. O'Connor, Targeting the DNA damage response in cancer, Mol. Cell. 60 (4) (2015) 547–560.
[63] C. Liu, C.E. Banister, C.C. Weige, D. Altomare, J.H. Richardson, C.M. Contreras, P. J. Buckhaults, PRDM1 silences stem cell-related genes and inhibits proliferation of human colon tumor organoids, Proc. Natl. Acad. Sci. Unit. States Am. 115 (22) (2018) E5066–E5075.
[64] R.S. Grigoryan, B. Yang, N. Keshelava, J.R. Barnhart, C.P. Reynolds, Flow cytometry analysis of single-strand DNA damage in neuroblastoma cell lines using the F7-26 monoclonal antibody, Cytometry Part A: The Journal of the International Society for Analytical Cytology 71 (11) (2007) 951–960.